Cell Research

www.nature.com/cr
www.cell-research.com

ARTICLE

Neddylation of PTEN regulates its nuclear import and promotes tumor development

Ping Xie[1], Zhiqiang Peng[2], Yujiao Chen[1], Hongchang Li[2], Mengge Du[1], Yawen Tan[3], Xin Zhang[2], Zhe Lu[4], Chun-Ping Cui[2], Cui Hua Liu[4], Fuchu He[2] and Lingqiang Zhang[2]

PTEN tumor suppressor opposes the PI3K/Akt signaling pathway in the cytoplasm and maintains chromosomal integrity in the nucleus. Nucleus–cytoplasm shuttling of PTEN is regulated by ubiquitylation, SUMOylation and phosphorylation, and nuclear PTEN has been proposed to exhibit tumor-suppressive functions. Here we show that PTEN is conjugated by Nedd8 under high glucose conditions, which induces PTEN nuclear import without effects on PTEN stability. PTEN neddylation is promoted by the XIAP ligase and removed by the NEDP1 deneddylase. We identify Lys197 and Lys402 as major neddylation sites on PTEN. Neddylated PTEN accumulates predominantly in the nucleus and promotes rather than suppresses cell proliferation and metabolism. The nuclear neddylated PTEN dephosphorylates the fatty acid synthase (FASN) protein, inhibits the TRIM21-mediated ubiquitylation and degradation of FASN, and then promotes de novo fatty acid synthesis. In human breast cancer tissues, neddylated PTEN correlates with tumor progression and poor prognosis. Therefore, we demonstrate a previously unidentified pool of nuclear PTEN in the Nedd8-conjugated form and an unexpected tumor-promoting role of neddylated PTEN.

Cell Research (2021) 31:291–311; https://doi.org/10.1038/s41422-020-00443-z

INTRODUCTION

PTEN encodes a membrane-bound protein phosphatase with potent tumor suppressor activity.[1–3] Loss of PTEN function leads to excessive activation of the PI3K/Akt oncogenic pathway, which stimulates cell growth and survival.[4–6] Recent studies have suggested that nuclear PTEN exhibits a complementary mechanism with cytoplasmic PTEN to suppress tumor development.[7] Nuclear PTEN interacts with centromeres to maintain their stability,[8] is involved in DNA repair,[9] and regulates gene transcription.[10–13] Mono-ubiquitination of PTEN by Nedd4 and deubiquitination by HAUSP/USP7 contribute to the regulation of the nuclear import and export of PTEN.[14,15] SUMOylation of PTEN also controls its nuclear localization. In cells exposed to genotoxic stress, SUMOylated PTEN was rapidly exported from the nucleus, a process that was dependent on the protein kinase ATM.[16]

Nedd8 is a ubiquitin-like protein that is covalently conjugated to substrates in a manner similar to ubiquitin.[17] The neddylation system consists of an activating enzyme (E1, a heterologous dimer composed of UBA3 and NAE1/APP-BP1), two conjugating enzymes (E2s, UBE2M/Ubc12 and UBE2F) and a variety of E3 ligases.[18] Neddylation primarily targets Cullin–RING ubiquitin ligases for their activation, and an increasing number of non-Cullin targets of Nedd8 have been identified. Neddylation can be removed by deneddylases, including NEDP1 and JAB1/CSN5.[19,20] An inhibitor of E1, named MLN4924 (also known as pevonedistat), has been evaluated in a series of phase I/II/III clinical trials both alone and in combination with chemo-/radiotherapies.[21,22] Overactive neddylation has been indicated to be closely correlated with cancer development.[23]

Abnormal cancer cell growth and survival depend on the demand for nutrients, including glucose, amino acids and lipids.[24] High levels of glucose and growth factors are reported to induce K27-linked polyubiquitination of PTEN, which alters PTEN phosphatase activity and promotes epithelial–mesenchymal transition.[25] However, it is poorly known whether there exist other post-translational modifications of PTEN in an environment with sufficient nutrients. Here, we report PTEN to be a genuine substrate of neddylation. High levels of glucose trigger PTEN neddylation and consequently induce PTEN nuclear import. Nuclear neddylated PTEN stabilizes fatty acid synthase (FASN) to promote tumor development, which indicates a novel cancer-promoting function of nuclear PTEN. Furthermore, PTEN neddylation accompanies and promotes the progression of human breast cancer. These data reveal that neddylation can switch PTEN from a tumor suppressor to a tumor promoter and provide a novel mechanism in neddylation-enhanced tumorigenesis.

RESULTS

PTEN is conjugated by Nedd8

To allow the proteomic identification of proteins modified with Nedd8, we first conducted affinity purification and mass spectrometry analysis to identify proteins that interact with Nedd8. In these experiments, Flag-tagged Nedd8 was stably expressed in

[1]Department of Cell Biology, The Municipal Key Laboratory for Liver Protection and Regulation of Regeneration, Capital Medical University, Beijing 100069, China; [2]State Key Laboratory of Proteomics, National Center for Protein Sciences (Beijing), Beijing Institute of Lifeomics, Beijing 100850, China; [3]Department of Breast and Thyroid Surgery, The Second People's Hospital of Shenzhen, Shenzhen, Guangdong 518035, China and [4]CAS Key Laboratory of Pathogenic Microbiology and Immunology, Institute of Microbiology (Chinese Academy of Sciences), Savaid Medical School, University of Chinese Academy of Sciences, Beijing 100101, China
Correspondence: Ping Xie (xiep@ccmu.edu.cn) or Lingqiang Zhang (zhanglq@nic.bmi.ac.cn)
These authors contributed equally: Ping Xie, Zhiqiang Peng

Received: 31 March 2020 Accepted: 29 October 2020
Published online: 9 December 2020

MCF-7 breast cancer cells. Whole-cell extracts were prepared and subjected to affinity purification using an anti-Flag affinity gel (Fig. 1a). Mass spectrometry analysis indicated that Nedd8 was copurified with NAE1 (APP-BP1), UBA3, Ubc12 (UBE2M), ribosomal proteins, and Cullins, all of which were previously reported to be enzymes or substrates of protein neddylation.[18] Surprisingly, PTEN, a tumor suppressor protein, was identified as one of these candidate proteins (Supplementary information, Fig. S1a and Data S1). Flag-tagged Nedd8 was coimmunoprecipitated with NAE1, UBA3, Ubc12, RPL7, Cullin4A and PTEN proteins from lysates of MCF-7 cells, which confirms this interaction (Fig. 1a). Importantly, PTEN was shown to interact with endogenous Nedd8 and NEDP1, a deneddylation enzyme, in cells but not with UBA3 or Ubc12 (Fig. 1b; Supplementary information, Fig. S1b).

To date, PTEN neddylation has never been reported in the literature. To further evaluate this modification, immunoprecipitation (IP) under partially denaturing conditions was performed with an anti-PTEN antibody, and the precipitates were detected as smear bands (Supplementary information, Fig. S1c). Mass spectrometry analysis of the smear bands revealed that endogenous PTEN was covalently bound to Nedd8 (Supplementary information, Data S2), suggesting that PTEN might be neddylated. When Nedd8 was ectopically expressed, PTEN migrated as high-molecular-weight bands (ubiquitin and SUMO2 were used as positive controls) (Fig. 1c). The smear bands were abolished in cells expressing Nedd8-ΔGG, a mutant incapable of covalently conjugating to its substrates (Fig. 1d), suggesting that the observed smear bands represent Nedd8-conjugated PTEN. We detected that two additional PTEN isoforms, PTENα and PTENβ,[26,27] could also be neddylated (Supplementary information, Fig. S1d). An in vivo assay further confirmed PTEN neddylation in MCF-7 and MDA-MB-231 cells (Supplementary information, Fig. S1e). The smear bands were eliminated by either treatment with the E1 inhibitor MLN4924 or deletion of *UBA3* (E1) or *Ubc12* (E2) using target sgRNAs (Fig. 1e, f; Supplementary information, Fig. S1f). Neddylated PTEN could not be recognized by the anti-ubiquitin antibody, and ubiquitinated PTEN was not recognized by the anti-Nedd8 antibody (Supplementary information, Fig. S1g). Moreover, knockout of *NEDP1* by sgRNA or knockdown of *NEDP1* by shRNA increased PTEN neddylation but did not change PTEN ubiquitination (Fig. 1g). Ectopic expression of wild-type (WT) NEDP1, but not the catalytically inactive C163A mutant, reduced PTEN neddylation (Supplementary information, Fig. S1h). By contrast, JAB1, a deneddylation enzyme responsible for the deneddylation of Cullins, had no significant effect on PTEN neddylation (Supplementary information, Fig. S1i). Furthermore, the levels of Nedd8-conjugated PTEN were significantly enhanced in multiple tissues of *NEDP1*$^{-/-}$ mice (Fig. 1h–k; Supplementary information, Fig. S1j). These observations suggest that NEDP1 is the specific deneddylase for PTEN.

Cullin proteins and Smurf1 have been identified as mono-neddylation substrates that target a single lysine or multiple lysine residues.[18,28] To date, the chain type of most neddylation substrates remains largely unclear. Nedd8 contains 8–9 lysine residues that can be used to form chains, and an unanchored tri-Nedd8 chain that could bind to PARP has been reported.[29,30] Poly-Nedd8 formation occurs only during cellular responses to stress,[30] and the lysine-null mutant Nedd8-K0 (all lysines were mutated to arginines) could prevent the formation of the poly-Nedd8 chain. As shown in Fig. 1l, high-molecular-weight bands of PTEN were observed in cells expressing WT Nedd8 (lane 2) but not in cells expressing either Nedd8-K0 or Nedd8-ΔGG (lanes 3 and 4, respectively), suggesting that PTEN was conjugated to poly-Nedd8 chains. We observed a specific band at 70 kDa in the Nedd8-K0 group, which was abolished by treatment with MLN4924 (lane 7), indicating that this band represented neddylated PTEN. Since the molecular weight of Nedd8 is 9 kDa, the specific band at 70 kDa suggests that PTEN was conjugated to two Nedd8 moieties (see Fig. 2; modification sites identified as K197 and K402). Next, we aimed to verify the molecular weight of neddylated and SUMOylated PTEN. The results in Fig. 1m show that immunoblotting with the PTEN antibody detected smear bands of a higher molecular weight and a specific band at approximately 70 kDa (left panel, lane 2). Only a specific band at 70 kDa was found when immunoblotting with a SUMO2/3 antibody (right panel, lane 2), and this band was hardly detectable in cells treated with the SUMOylation inhibitor 2-D08 (lane 4 of both the left and right panels); this indicates that the 70 kDa band represents SUMOylated PTEN. This is consistent with a previous report.[16] Moreover, the high-molecular-weight smear bands larger than 70 kDa were eliminated upon MLN4924 treatment (left panel, lane 3). These bands could also be detected by anti-Nedd8 antibody (middle panel). Collectively, neddylated PTEN is larger than 70 kDa, as indicated by the smear bands of a higher molecular weight. These results suggest that Nedd8 forms a covalent poly-chain on the PTEN protein, which induces a visible shift in the molecular weight of PTEN.

XIAP serves as a ligase of PTEN neddylation at K197 and K402

We next determined which E3 ligase is involved in PTEN neddylation. It has been reported that many substrates of Nedd8 and ubiquitin share the same E3 ligase.[18,31] Our data showed that only the depletion of *XIAP*, which has been identified as a Nedd8 ligase for caspases[32] and a ubiquitin ligase for PTEN,[33] effectively decreased PTEN neddylation, whereas the loss of other ubiquitin ligases for PTEN, including Nedd4-1,[34] WWP1[35] and WWP2,[36] did not affect PTEN neddylation (Fig. 2a; Supplementary information, Fig. S2a). In addition, except for XIAP, depletion of endogenously expressed known Nedd8 ligases, including Mdm2,[37] c-Cbl,[38] and Roc1,[39] did not change PTEN neddylation (Fig. 2b). An in vitro PTEN neddylation assay further indicated that XIAP catalyzed PTEN neddylation (Supplementary information, Fig. S2b), and this modification was removed by the introduction of purified NEDP1 (Fig. 2c). Depletion of *XIAP* in breast cancer cell lines markedly decreased PTEN neddylation (Supplementary information, Fig. S2c, d), whereas treatment with Embelin, an inhibitor of XIAP,[40,41] eliminated PTEN neddylation (Supplementary information, Fig. S2e). Furthermore, ubiquitination of the catalytically inactive H476A mutant of XIAP could not attach Nedd8 onto PTEN (Fig. 2d). PTEN-4A (mutations of Ser380, Thr382, Thr383, and Ser386 to alanine), a phosphorylation-deficient mutant,[42] was more heavily modified by neddylation than PTEN-WT, while the neddylation levels of PTEN-4E and PTEN-WT did not show major difference (Supplementary information, Fig. S2f). These results indicate that XIAP is likely the major Nedd8 E3 ligase of PTEN.

PTEN protein contains a total of 34 lysine residues (Fig. 2e). To determine the Nedd8 acceptor sites in PTEN, individual K-R mutants and a K0 mutant (all 34 lysines mutated to arginines) were generated. We found that PTEN proteins with K197R and K402R mutations had reduced PTEN neddylation (Fig. 2f). The double mutant K197/402R (referred to as 2KR) exhibited nearly no neddylation (Fig. 2g), suggesting that K197 and K402 are the major sites for neddylation of PTEN. In vitro neddylation assays confirmed this conclusion (Fig. 2h; Supplementary information, Fig. S2g). Notably, the 2KR mutation did not affect PTEN ubiquitination (Supplementary information, Fig. S2h). The K402 site is located within the C-terminal PDZ-binding domain of PTEN. To test whether PTEN neddylation affects the interaction with PDZ proteins, computer simulations were first conducted, and they showed that the K402R mutation did not affect the PTEN structure (Supplementary information, Fig. S2i). Then, a definitive structure of the neddylated PTEN was presented to speculate the possible changes in its interaction with MAST2, a PDZ protein known to bind PTEN[43] (Supplementary information, Fig. S2j, k). The results showed that neddylated PTEN at the K402 site no longer interacted with MAST2 (Supplementary information,

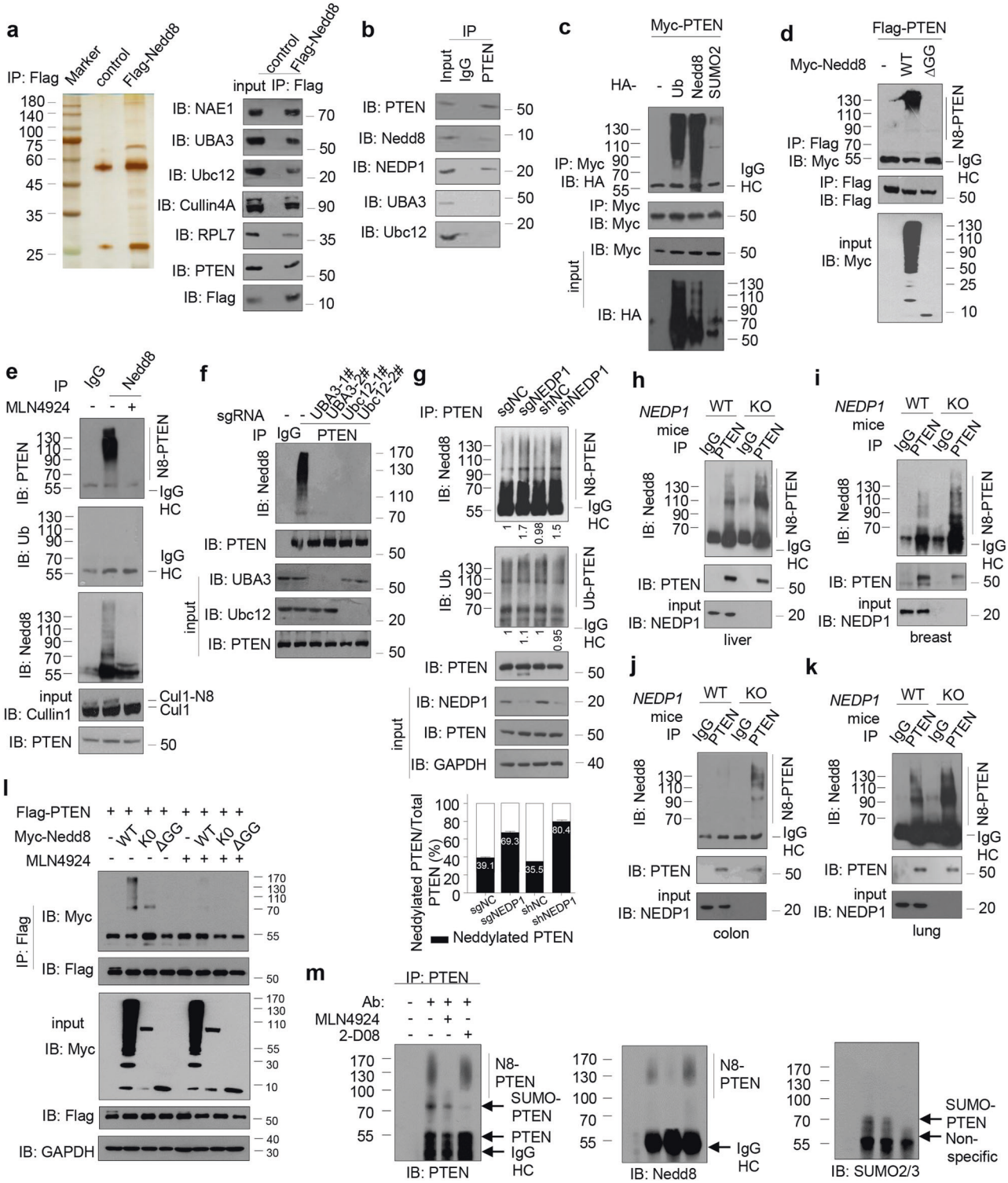

Fig. 1 Nedd8 covalently interacts with PTEN. a Cellular extract from MCF-7 cells stably expressing Flag (control) or Flag-Nedd8 were immunopurified with anti-Flag antibody and then eluted. The eluates were resolved by SDS-PAGE and silver-stained. The protein bands were retrieved and analyzed by mass spectrometry. Immunopurified proteins were analyzed by western blotting using antibodies against the indicated proteins. **b** Immunoblot of anti-PTEN immunoprecipitate from MCF-7 cells. **c**, **d** Immunoblot of anti-Myc (**c**) or anti-Flag (**d**) immunoprecipitate and whole cell lysate (WCL) from MCF-7 cells transfected with indicated constructs. **e**, **f** PTEN neddylation was attenuated by MLN4924 (1 μM, 12 h), or deletion of *UBA3* or *Ubc12*. Immunoblot analysis of anti-Nedd8 (**e**) or anti-PTEN (**f**) immunoprecipitate and WCL from MCF-7 cells. **g**–**k** PTEN neddylation was enhanced by the deletion or depletion of *NEDP1*. Immunoblot analysis of anti-PTEN immunoprecipitate and WCL from MCF-7 cells (**g**), or tissues of *NEDP1* WT and KO mice (**h**–**k**). The ratio of neddylated PTEN over total PTEN was quantified (**g**). **l** Immunoblot of anti-Flag immunoprecipitate and WCL from MCF-7 cells transfected with indicated constructs. The cells were treated with MLN4924 (1 μM, 12 h) before harvested. **m** PTEN was immunoprecipitated from MCF-7 cells with protein A beads (Ab) alone or anti-PTEN antibody (CST #9559) and immunoblotted with the anti-PTEN antibody (CST #9188) then stripped and re-probed with antibodies to Nedd8 and SUMO2/3.

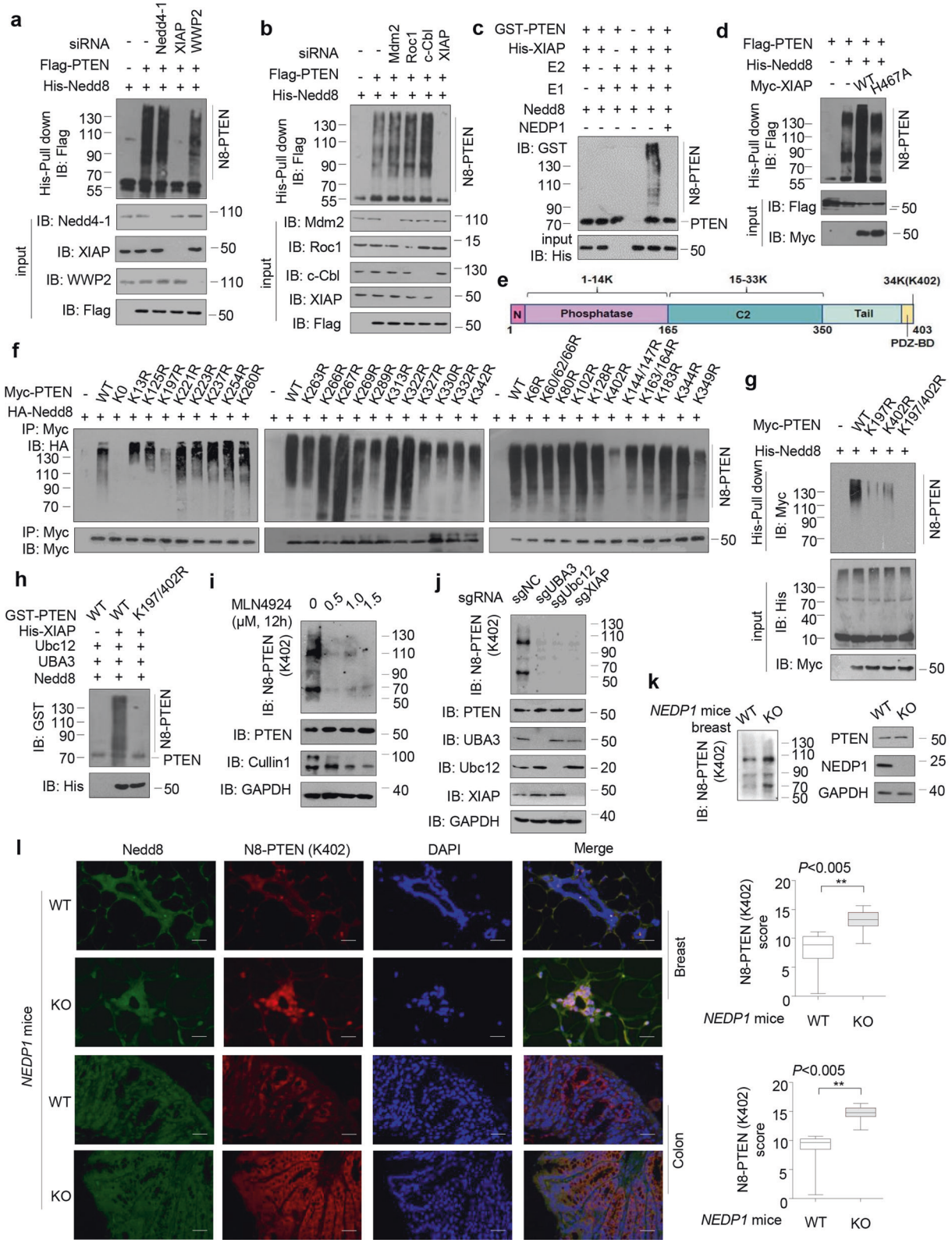

Fig. S2l, m). We assume that neddylation might alter the conformation of the PTEN C-terminus and prevent the insertion of the PTEN C-terminal motif into the PDZ pocket.

Considering that the K197 residue on PTEN is surrounded by hydrophobic amino acids, it is difficult to generate a specific antibody targeting this site. Thus, we generated an antibody that was specific to the K402-neddylated PTEN protein but not to either ubiquitinated or SUMOylated PTEN (Supplementary information, Fig. S2n). Endogenous PTEN neddylation on K402 was abrogated by treatment with increasing concentrations of MLN4924 (Fig. 2i) as well as the deletion of *UBA3*, *Ubc12*, or *XIAP* (Fig. 2j). Compared with the WT mice, *NEDP1*$^{-/-}$ mice showed

Fig. 2 XIAP promotes PTEN neddylation on K197 and K402. a, **b** Immunoblot analysis of Ni-NTA pull-downs or WCL from MCF-7 cells with the depletion of *Mdm2*, *Roc1*, *c-Cbl*, *Nedd4-1*, *WWP2* and *XIAP*. **c** In vitro covalent neddylation of PTEN. Purified His-XIAP and GST-PTEN proteins were incubated with Nedd8, Nedd8-E1/E2, NEDP1. Reactions were performed as described in the Materials and methods section. Samples were analyzed by western blotting with indicated antibodies. **d** Immunoblot analysis of Ni-NTA pull-downs or WCL from MCF-7 cells transfected with indicated constructs. **e** A schematic diagram of the lysine sites on PTEN is shown. **f**, **g** PTEN neddylation occurred on K197 and K402. Immunoblot analysis of anti-Myc immunoprecipitate, Ni-NTA pull-downs and WCL from MCF-7 transfected with indicated constructs. **h** Purified His-XIAP and GST-PTEN WT or 2KR proteins were incubated with Nedd8, Nedd8-E1/E2. Reactions were performed and analyzed by western blotting. **i**, **j** Treatment of MLN4924, or the deletion of *UBA3*, *Ubc12*, *XIAP* decreased PTEN neddylation on K402. Immunoblot of WCL from MCF-7 cells with MLN4924 treatment (**i**), or *UBA3*-, *Ubc12*-, *XIAP*-deleted MCF-7 cells (**j**). **k** Deletion of *NEDP1* increased PTEN neddylation on K402. Immunoblot of WCL from breast tissues of WT or *NEDP1* KO mice. **l** Immunofluorescent of Nedd8 and neddylated PTEN (K402) in breast or colon tissues of WT or *NEDP1* KO mice. Scale bar, 25 μm. The level of PTEN neddylation scores are shown as box plots. Data were analyzed using the Student's *t*-test.

elevated PTEN neddylation on K402 (Fig. 2k, l). Collectively, these data support a critical role of XIAP and NEDP1 in PTEN neddylation at K197 and K402.

Neddylation promotes PTEN nuclear import

Considering that PTEN inhibits the PI3K/Akt signaling pathway to suppress cell survival and proliferation, we attempted to explore the activity of the PI3K/Akt signaling pathway when PTEN is neddylated. Ectopic expression of PTEN decreased phospho-Akt levels as well as the levels of phosphorylation of Akt downstream targets, such as mTOR, S6K and 4E-BP1, without affecting their total protein levels; furthermore, MLN4924 treatment significantly enhanced this effect (Fig. 3a). Overexpression of Nedd8 led to earlier activation and prolonged duration of insulin-induced PI3K/Akt signaling pathway activity (Supplementary information, Fig. S3a). Additionally, the patterns of the levels of phospho-Akt and its downstream targets were clearly enhanced in different tissues of *NEDP1*$^{-/-}$ mice and in *NEDP1*-knockout cells, and MLN4924 treatment ameliorated this effect (Fig. 3b, c). LY294002, an inhibitor of PI3K/Akt signaling, did not affect PTEN neddylation (Supplementary information, Fig. S3b). Taken together, these data support the notion that PTEN neddylation enhances the activity of the PI3K/Akt signaling pathway.

To elucidate the mechanism of how PTEN neddylation promotes PI3K/Akt signaling pathway activity, we first examined PTEN expression and found that neddylation did not contribute to PTEN stability. Neither overexpression or knockdown of Nedd8 nor treatment with MLN4924 affected the protein stability of PTEN (Supplementary information, Fig. S3c–e). Moreover, neddylation did not affect PTEN phosphatase activity (Supplementary information, Fig. S3f). Interestingly, we observed that in the absence of ectopic Nedd8, PTEN was localized to both the cytoplasm and nucleus (cells indicated by white arrows in Fig. 3d, left). Strikingly, in cells expressing ectopic Nedd8, PTEN was predominantly localized to the nucleus (cells indicated by white arrowheads in Fig. 3d, left, e; Supplementary information, Fig. S3g). Assessment of protein levels in the nuclear and cytoplasmic fractions showed a clear enrichment of nuclear PTEN in Nedd8-overexpressing cells (Fig. 3f). Conversely, MLN4924 sequestered the majority of PTEN to the cytoplasm (Fig. 3d, right, e, f). Furthermore, we analyzed the effect of *NEDP1* deletion on PTEN localization. In parental cells, PTEN was distributed throughout the cell; however, the proportion of nuclear PTEN was enriched in *NEDP1*-deleted cells (Fig. 3g–i). Finally, GFP-PTEN 2KR mutant proteins accumulated in the cytoplasm of MCF-7 cells (Fig. 3j–l). These data suggest that neddylation promotes PTEN nuclear translocation.

p53-Nedd8 is predominantly localized in the nucleus.[37] It has been demonstrated that SCCRO enhances Cullin1 neddylation and nuclear import,[44] whereas MLN4924 induces FOXO3a nuclear export.[45] Neddylation tends to control the subcellular localization of its substrates, but the mechanism involved remains completely unknown. Nuclear protein import requires the nuclear pore-targeting complex, which includes importin proteins.[46] We noticed that more than one importin protein was identified as a potential Nedd8-interacting protein (Supplementary information, Fig. S1a). Indeed, Nedd8 was coimmunoprecipitated with importin α, importin β, and IPO5 but not with IPO4 (Fig. 3m), and ectopic expression of Nedd8 promoted the interaction of importin with WT-PTEN but not with the neddylation-deficient 2KR PTEN mutant (Fig. 3n), suggesting that neddylation mediates the binding of importin to PTEN. These data provide a potential mechanism of how neddylation promotes PTEN nuclear translocation.

PTEN neddylation is induced under high concentrations of glucose

Post-translational modification of proteins always occurs under specific physiological conditions. Previous studies have shown that when cells are exposed to genotoxic stressors, SUMOylation influences the nucleus–cytoplasm shuttling of PTEN, and nuclear SUMOylated PTEN plays a role in the DNA damage response.[16] High levels of glucose and growth factors induce K27-linked polyubiquitination of PTEN and direct the PTEN phosphatase switch.[25] To elucidate the physiological relevance of PTEN neddylation, we established an endogenous PTEN modification assay under different stressors, including DNA damage (MMS, cisplatin), cold/heat shock, nutrient deprivation (serum-free conditions; the glycolysis inhibitor 2-deoxy-D-glucose (2-DG)), oxidative stress (H_2O_2) and hypoxia (1% O_2). Interestingly, we found that only 2-DG specifically decreased the levels of PTEN neddylation (Fig. 4a; Supplementary information, Fig. S4a). Glucose-derived production of acetyl-CoA is tightly linked with protein acetylation.[47] As expected, 2-DG treatment inhibited PTEN acetylation but not PTEN SUMOylation (Fig. 4a). We further found that PTEN neddylation was increased with increasing levels of glucose in a dose-dependent manner (Fig. 4b) but decreased with time-dependent deprivation of glucose (Supplementary information, Fig. S4b). PTEN neddylation was detected one hour after glucose was added (Supplementary information, Fig. S4c). The half-life of PTEN neddylation in cultured mammalian cells was approximately 6 h (Supplementary information, Fig. S4d). Furthermore, PTEN neddylation was examined in *db/db* mice (a model of diabetes), which have pathologically high levels of glucose. Our data showed that the endogenous PTEN neddylation levels in multiple tissues were higher in the elderly model mice than in the younger model mice, which were correlated with the progressing diabetic phenotypes in *db/db* mice (Supplementary information, Fig. S3e–g). Importantly, PTEN neddylation levels were relatively higher in *db/db* mouse tissues than in WT mouse tissues (Fig. 4c). The PTEN K402 site has been reported to be acetylated by CBP.[48] Our data showed that glucose increased the levels of both K402-Nedd8 and acetyl-PTEN (Fig. 4d). However, we noticed that PTEN K402 acetylation occurred under low glucose concentration (5 mM) while PTEN K402 neddylation required higher glucose concentrations (10 mM and 25 mM). It seemed that the glucose level directs the acetylation or neddylation of PTEN at the K402 site. MLN4924 had a minimal effect on PTEN K402 acetylation (Supplementary information, Fig. S4h), and ICBP112, an inhibitor of CBP acetyltransferase, did not affect PTEN neddylation (Supplementary information, Fig. S4i, j). By contrast,

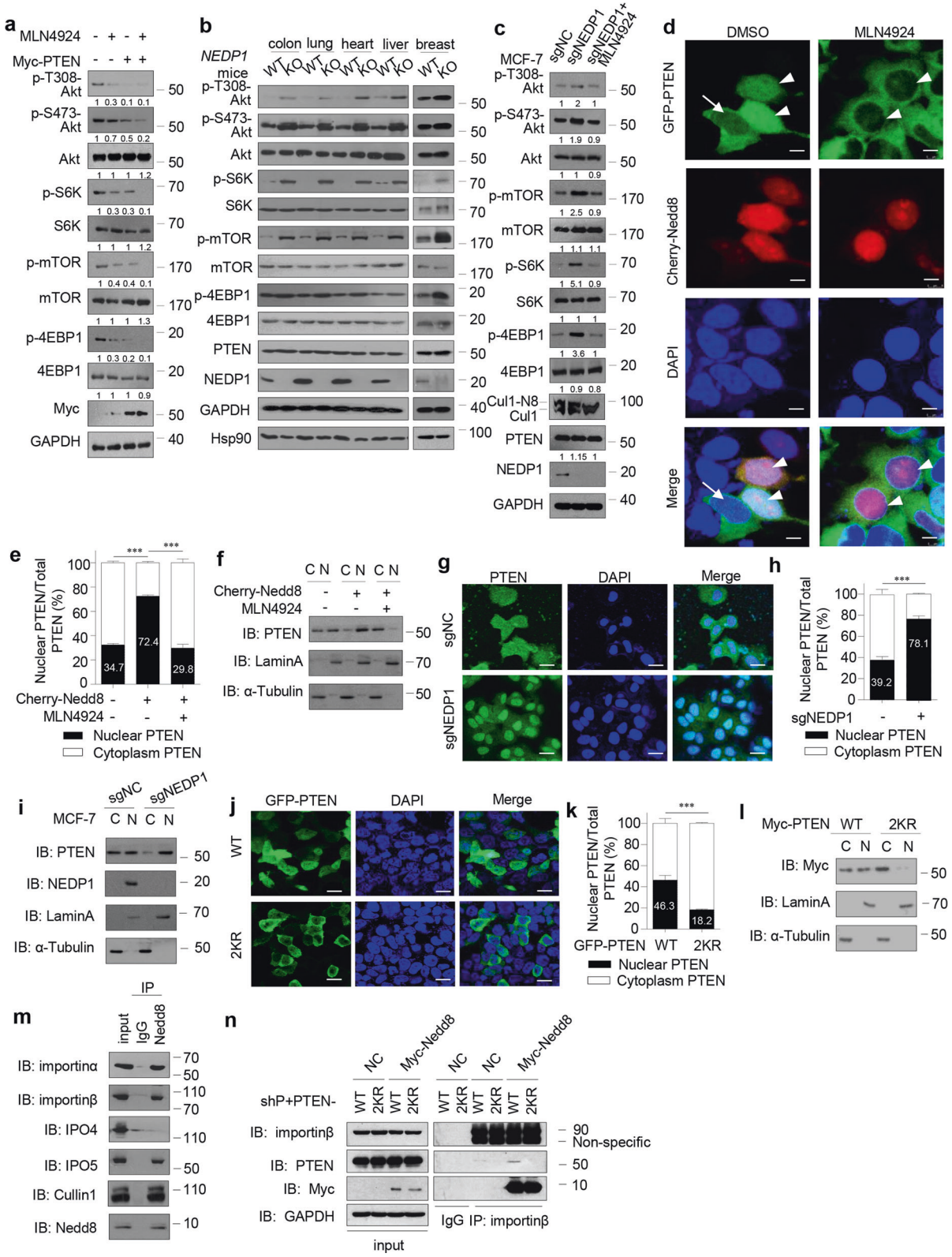

MLN4924 treatment maintained PTEN localization to the cytoplasm, and ICBP112 did not change the localization of PTEN (Supplementary information, Fig. S4k, l). ICBP112 treatment inhibited the interaction of PTEN with PDZ proteins, such as Dlg5 and Magi2[48]; however, MLN4924 did not affect such interactions (Supplementary information, Fig. S4m). These results suggest that PTEN neddylation preferentially regulates the cytoplasmic-nuclear localization of PTEN, whereas PTEN acetylation (on K402) preferentially regulates the interactions with plasma membrane-associated PDZ proteins.

Given that PTEN neddylation is influenced by the glucose concentration, we sought to determine whether glucose levels

Fig. 3 Neddylation promotes PTEN nuclear import and enhances PI3K/Akt signaling pathway. a–c Neddylation enhances PI3K/Akt activation. Immunoblot of WCL from MCF-7 cells transfected with Myc-PTEN (**a**), or tissues of WT or *NEDP1* KO mice (**b**), or *NEDP1*-deleted MCF-7 cells (**c**). The cells were treated with 1 μM MLN4924 for 12 h. **d** Immunofluorescence analysis of GFP-PTEN (green) and Cherry-Nedd8 (red) in MCF-7 cells. White arrow head points to Cherry-Nedd8 and GFP-PTEN co-expressed cells. White arrow points to the cells in which only GFP-PTEN expressed. All images were identically processed and used the same scale bar (10 μm). Cells were treated with 1 μM MLN4924 for 12 h. **e** An average (%) of 100 cells was counted for quantification of GPF-PTEN localization in three independent experiments. Error bars, ± SD. ***$P < 0.001$. **f** Immunoblot of Nuclear (N) vs Cytoplasmic (C) fractionation from MCF-7 cells transfected with Cherry-Nedd8. **g** Immunofluorescence of PTEN in MCF-7 cells with *NEDP1* knockout. Scale bar, 25 μm. **h** An average (%) of 100 cells was counted for quantification of PTEN localization in three independent experiments. Error bars, ± SD. ***$P < 0.001$. **i** Immunoblot of Nuclear (N) vs Cytoplasmic (C) fractionation from *NEDP1*-deleted MCF-7 cells. **j** Immunofluorescence of GFP-PTEN WT and 2KR in MCF-7 cells. Scale bar, 25 μm. **k** An average (%) of 100 cells was counted for quantification of GPF-PTEN WT and 2KR cellular localization in three independent experiments. Error bars, ± SD. ***$P < 0.001$. **l** Immunoblot of Nuclear (N) vs Cytoplasmic (C) fractionation from MCF-7 cells transfected with indicated constructs. **m** Immunoblot analysis of anti-Nedd8 immunoprecipitate and WCL from MCF-7 cells. **n** Immunoblot analysis of anti-importinβ immunoprecipitate and WCL from MCF-7 cells transfected with indicated constructs.

affect the subcellular localization of PTEN. In cells deprived of glucose, neddylated PTEN was undetectable, and PTEN mainly localized to the cytoplasm (Fig. 4e, left; f, lanes 1 and 4, long exposure). When glucose was added to the cultures, neddylated PTEN levels increased, and the protein was primarily localized to the nucleus (Fig. 4e, right, f, lanes 2 and 5, long exposure). Treatment with MLN4924 decreased neddylated PTEN in the nucleus (Fig. 4f, lanes 3 and 6, long exposure), and PTEN nuclear export increased with gradual decreases in glucose levels (Supplementary information, Fig. S4n–p). Importantly, the glucose-mediated nuclear import of neddylated PTEN was abolished by the deletion of *UBA3, Ubc12* or *XIAP* (Supplementary information, Fig. S5a–d). By contrast, deletion of *NEDP1* further increased the nuclear enrichment of neddylated PTEN (Fig. 4g, h). To better understand the dynamic translocation of PTEN upon glucose stimulation, we performed live-cell imaging. Cells were initially deprived of glucose for 12 h before it was added for 8 h. We observed that PTEN-WT gradually translocated from the cytoplasm to the nucleus (Fig. 4i; Supplementary information, Video S1) but that PTEN 2KR was retained within the cytoplasm (Fig. 4i; Supplementary information, Video S2). Similar results were obtained in *PTEN*-depleted cells ectopically expressing resistant PTEN-WT or 2KR (Fig. 4j, k). These results suggest that in the presence of high concentrations of glucose, neddylation promotes the nuclear translocation of PTEN.

Next, we intended to elucidate the time course of PTEN translocation and PTEN neddylation. Cells were first deprived of glucose for 12 h before it was added back to the culture medium. After glucose stimulation, neddylated PTEN was detectable as early as 1 h (Fig. 4l, lanes 3 and 4). At this timepoint, both PTEN and neddylated PTEN were detected in the cytoplasm rather than the nucleus. One hour later, both PTEN and neddylated PTEN were detectable in both the cytoplasm and the nucleus (Fig. 4l, lanes 5 and 6). The accumulation of unmodified and neddylated PTEN proteins in the nucleus continued to increase until, at 12 h after glucose treatment, almost all PTEN proteins were distributed in the nucleus (Fig. 4l, lanes 7–12). These results clearly indicate that PTEN neddylation occurred first in the cytoplasm before accumulating in the nucleus. Collectively, these results provide convincing evidence that high levels of glucose stimulate PTEN neddylation, which further promotes the nuclear localization of PTEN.

We sought to explore the underlying mechanism by which glucose controls the neddylation of PTEN. Strikingly, the protein levels of UBA3 and Ubc12, but not those of NEDP1, were distinctly upregulated with increasing glucose concentrations (Supplementary information, Fig. S5e); however, glucose did not change the subcellular localization of UBA3 and Ubc12 (Supplementary information, Fig. S5f). Notably, glucose enhanced the mRNA transcription of *UBA3* and *Ubc12* (Supplementary information, Fig. S5g). Although the precise mechanism needs further investigation, the current results suggest that high levels of glucose induce neddylation via upregulation of the transcription of neddylation enzymes, at least in part.

PTEN neddylation promotes tumorigenesis

Next, we explored the role of PTEN neddylation in tumorigenesis. A fusion protein (PTEN-Nedd8) was generated by linking Nedd8 to the C-terminus of PTEN to mimic neddylated PTEN. As a comparison, a nuclear localization sequence (NLS) was fused to the N-terminus of PTEN (NLS-PTEN) as described in a previous study.[49] We generated stably transduced MCF-7 breast cancer cells and MCF-10A mammary epithelial cells by performing lentiviral transduction with Lenti-shNC (negative control), Lenti-shPTEN, and shPTEN co-transfected with resistant PTEN constructs, including PTEN-WT, PTEN-2KR, NLS-PTEN or PTEN-Nedd8 (Supplementary information, Fig. S6a, b). *PTEN* depletion enhanced the phosphorylation levels of Akt and its downstream targets, such as mTOR, S6K and 4EBP1, without affecting their total protein levels (Fig. 5a, b, lanes 1 and 2). Ectopic expression of PTEN-WT reversed these effects (lane 3), but ectopically expressed PTEN-Nedd8 had no such effect (Fig. 5a, lane 4). PTEN-C124S-Nedd8, which can neither integrate into the lipid membrane nor exert protein phosphatase activity, worked as well as did PTEN-Nedd8 (Fig. 5a, lane 5). PTEN-2KR showed more significant effects than PTEN-WT (Fig. 5b). Strikingly, PTEN-Nedd8 accelerated cell proliferation, colony formation, and cell migration, whereas PTEN-WT, PTEN-2KR and NLS-PTEN exhibited suppressive effects (Fig. 5c–e). PTEN-Nedd8 showed a stronger effect on promoting tumor cell growth in a xenograft nude mouse model; by contrast, PTEN-2KR markedly suppressed tumor growth and was more effective than PTEN-WT (Fig. 5f±i).

In addition, PTEN-Nedd8 obviously promotes cell proliferation and migration in MCF-10A cells (Fig. 5j, k), which ultimately displayed severe signs of senescence defects (Supplementary information, Fig. S6c). PTEN-Nedd8 promoted migration by upregulating Vimentin and Snail and downregulating E-cadherin, and PTEN-2KR exhibited opposing effects (Fig. 5l). Moreover, overexpression of XIAP markedly enhanced tumor cell proliferation and migration in cells expressing PTEN-WT but not in cells expressing PTEN-2KR (Fig. 5m–o), suggesting that XIAP exhibited oncogenic effects through neddylation of PTEN, at least in part. To further investigate the potential tumor-promoting function of PTEN neddylation in vivo, we constructed a knock-in (KI) MCF-7 cell line with $PTEN^{2KR}$ mutants (Supplementary information, Fig. S6d). Compared with WT MCF-7 cells, $PTEN^{2KR}$ KI cells showed decreases in both PTEN neddylation and PI3K/Akt pathway activity (Fig. 5p). Furthermore, $PTEN^{2KR}$ KI cells exhibited a notable tumor-suppressive effect on cell proliferation, colony formation, cell migration and tumor growth in xenografted nude mice (Fig. 5q–v; Supplementary information, Fig. S6e). Taken together, these results indicate the tumor-promoting function of neddylated PTEN (K197/K402).

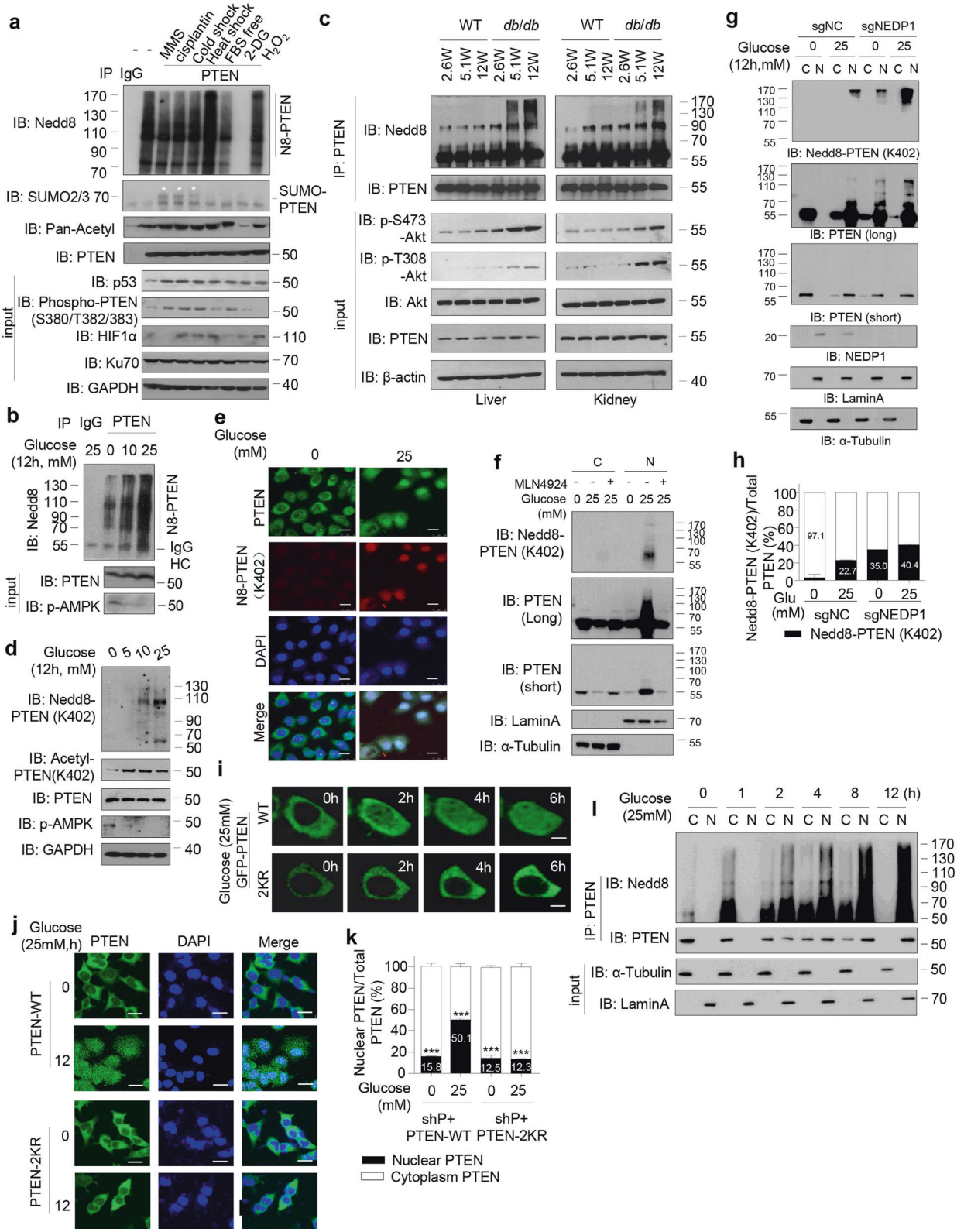

Neddylated PTEN increases the protein stability of fatty acid synthase

Next, we aimed to elucidate the underlying mechanism of PTEN-Nedd8 in tumorigenesis. Nuclear PTEN is essential for tumor suppression[49] and plays multiple roles, including binding to CENP-C to control genomic stability,[8] regulating the APC/C-CDH1 tumor-suppressive complex,[13] interacting with RAD51 and Ku70 to aid in DSB DNA repair,[50] and cooperating with E2F1 to influence chromatin remodeling.[51] Here, our results also confirmed these findings, and the reported interactions were reproducible with both PTEN-WT and NLS-PTEN (Supplementary information, Fig. S7a, lanes 2 and 3). However, the interaction of PTEN-Nedd8

Fig. 4 Neddylation controls PTEN subcellular localization upon glucose addition or deprivation. a Immunoblot analysis of anti-PTEN immunoprecipitate and WCL from MCF-7 cells. MCF-7 cells were treated with MMS (0.2 mM, 1 h), or cisplatin (1 μM, 12 h), or cold shock (4 °C for 30 min, then 37 °C for 4 h), or heat shock (45 °C for 30 min, then 37 °C for 4 h), or serum-starved for 4 h, or 2-DG (5 μM, 24 h), or H_2O_2 (800 μM, 30 min) before harvested. **b**–**d** Glucose promotes PTEN neddylation. Immunoblot analysis of anti-PTEN immunoprecipitate and WCL from MCF-7 cells cultured in cell medium containing different glucose concentrations (**b**, **d**), or diverse tissues of *db/db* diabetic mice at different age (**c**). **e** Immunofluorescence of PTEN and neddylated PTEN on K402 in MCF-7 cells. Scale bar, 25 μm. **f**–**h** Immunoblot of Nuclear (N) vs Cytoplasmic (C) fractionation from MCF-7 cells with MLN4924 treatment (1 μM, 12 h) (**f**), or *NEDP1* deletion (**g**), and the ratio of neddylated PTEN over total PTEN in **g** was quantified (**h**). The cells were cultured with different glucose concentrations. **i** Time-lapse images of GFP-PTEN WT or 2KR in HEK293T cells. The cells were first deprived of glucose in the culture medium and then stimulated with glucose (25 mM). Live cell imaging was performed to indicate the localization of GFP-PTEN WT or 2KR. Representative images of the indicated timepoints are shown. Scale bar, 10 μm. **j** Immunofluorescence of PTEN in shPTEN-resistant PTEN-WT and 2KR stable MCF-7 cells. Cells were deprived of glucose and followed by glucose stimulation (25 mM). Scale bar, 25 μm. **k** An average (%) of 100 cells was counted for quantification of PTEN localization in three independent experiments. Error bars, ± SD. ***$P < 0.001$. **l** Immunoblot of anti-PTEN immunoprecipitate from Nuclear (N) vs Cytoplasmic (C) fractionation. Glucose was removed for 12 h and then retreated with the indicated times.

with known nuclear partners was reduced (Supplementary information, Fig. S7a, lane 4). To identify proteins that interact with nuclear neddylated PTEN, the nuclear fractions of shPTEN + PTEN-Nedd8 stable MCF-7 cells were subject to IP followed by mass spectrometry analysis. FASN, a critical enzyme in fatty acid synthesis,[52,53] was identified as a candidate (Supplementary information, Fig. S7b). IP analysis further indicated that compared with NLS-PTEN, PTEN-Nedd8 showed a higher affinity for FASN and a lower affinity for Ku70 (Fig. 6a) as well as significantly enhanced FASN protein levels (Fig. 6b, c), while the mRNA level of FASN was unaffected (Supplementary information, Fig. S7c). The half-life of FASN protein was prolonged in the PTEN-Nedd8 stable cell line (Fig. 6d). Furthermore, PTEN-Nedd8 reduced the levels of ubiquitinated FASN (Fig. 6e; Supplementary information, Fig. S7d), whereas MLN4924 treatment resulted in decreased FASN protein levels (Supplementary information, Fig. S7e) and increased FASN ubiquitination (Supplementary information, S7f, lane 3). PTEN-2KR showed the opposite effect as PTEN-Nedd8 (Supplementary information, Fig. S7f, lanes 6 and 7). TRIM21 is known as a major E3 ubiquitin ligase of FASN.[53] Here, our data showed that PTEN-Nedd8 but not NLS-PTEN reduced the association of FASN with TRIM21 (Fig. 6f). To better illustrate the competition mechanism, a ternary coimmunoprecipitation assay was performed. The results indicated that in the presence of high levels of glucose, FASN favored the interaction with PTEN but not with TRIM21 (Fig. 6g–i). Upon glucose deprivation, FASN favored the interaction with TRIM21 but not PTEN (Fig. 6g–i). There was no interaction between PTEN and TRIM21 (Fig. 6h, i). FASN showed higher affinity for PTEN-Nedd8 and lower affinity for PTEN-2KR (Supplementary information, Fig. S7g, h). In addition, FASN activity was enhanced by PTEN-Nedd8 but inhibited by PTEN-2KR (Fig. 6j). Under high glucose concentrations, the protein stability of FASN was lower in $PTEN^{2KR}$ cells than in $PTEN^{WT}$ cells, while the levels of ubiquitinated FASN were higher in $PTEN^{2KR}$ cells (Fig. 6k). FASN colocalized with PTEN and Nedd8 in the cytoplasm and nucleus. However, upon glucose deprivation, both PTEN and FASN translocated to the cytoplasm and no longer colocalized with nuclear Nedd8 (Supplementary information, Fig. S7i–k). PTEN-Nedd8 increased the protein levels of both cytoplasmic and nuclear FASN (Fig. 6l), and PTEN-Nedd8 interacted with FASN in the nucleus (Fig. 6m). Remarkably, we noticed that PTEN-C124S-Nedd8 did not enhance FASN protein stability (Fig. 6n), suggesting that the phosphatase activity of PTEN is required for neddylated PTEN to stabilize FASN. Interestingly, PTEN-Nedd8, but not PTEN-C124S-Nedd8, decreased the tyrosine phosphorylation and ubiquitination of FASN and prevented the association of FASN with TRIM21 (Fig. 6o). Further cell fractionation analysis showed that PTEN-Nedd8 inhibited the tyrosine phosphorylation of FASN in the nucleus but not in the cytoplasm (Fig. 6p, lanes 9 and 10). PTEN-2KR showed the opposite effect as PTEN-Nedd8 (Fig. 6p, lanes 7 and 8). Collectively, these data suggest that neddylated PTEN in the nucleus dephosphorylates FASN, attenuates the interaction between FASN and TRIM21 and then upregulates the protein level and activity of FASN. FASN is essential for de novo fatty acid synthesis to support cancer cell growth.[52] Fatty acid analysis revealed that PTEN-Nedd8 elevated the level of total fatty acids compared to those in the control groups (Fig. 6q, r). Hence, we conclude that nuclear neddylated PTEN increases the stability of fatty acid synthase and promotes tumor cell proliferation.

PTEN neddylation promotes breast cancer progression

To better illustrate the effect of PTEN neddylation on tumor development, we monitored MMTV-*PyMT* mice starting 63 days after birth, which is when the mice began to spontaneously develop breast tumors, and then sacrificed them to measure the levels of neddylated PTEN in the tumor tissues. We observed that PTEN neddylation gradually increased in the following 14 days with the tumor growth process (Fig. 7a). Next, we prepared and injected shNEDP1-AAV into MMTV-*PyMT* mice to deplete *NEDP1* in vivo. Our data showed that *PyMT*/shNC-AAV mice spontaneously developed breast tumors at 80–84 days after birth, but the *PyMT*/shNEDP1-AAV mice first showed signs of the earliest breast tumors at 70–72 days (Fig. 7b, c; Supplementary information, Fig. S8a, b). The volume and weight of tumor tissues from *PyMT*/shNEDP1-AAV mice were significantly larger than those from *PyMT*/shNC-AAV mice (Fig. 7d, e). The levels of neddylated PTEN and the activity of the PI3K/Akt signaling pathway were notably increased in *PyMT*/shNEDP1-AAV mice (Fig. 7f). We observed that covalently conjugated Nedd8 was detected in nuclear PTEN but not in cytoplasmic PTEN (Fig. 7g, h).

Next, we explored the role of PTEN neddylation in facilitating tumorigenesis in an in vivo microenvironment with high glucose concentrations. We generated stably transduced murine 4T1 breast carcinoma cells via lentiviral infections with Lenti-shNC, Lenti-shPTEN, or shPTEN in conjunction with resistant PTEN constructs, including PTEN-WT and PTEN-2KR. Then, the indicated cells were inoculated into *db/db* mice and control mice. Overall, the growth rate and size of tumors in each group from *db/db* mice were significantly larger than those of control mice. Importantly, PTEN-2KR markedly suppressed tumor growth to a greater extent than PTEN-WT (Fig. 7i–k; Supplementary information, Fig. S8c). These data indicate that under pathologically high glucose levels, PTEN neddylation plays a role in facilitating tumorigenesis.

PTEN neddylation positively correlates with the progression of human breast cancer

Next, we investigated the role of PTEN neddylation at the clinical level. It has been well established that there is a 30%–40% reduction in PTEN protein expression in breast carcinoma.[54] Consistently, we confirmed that PTEN expression was significantly decreased in tumor tissues compared with matched adjacent normal tissues (Supplementary information, Fig. S9a, b). To better illustrate the effect of PTEN neddylation on tumorigenesis, we detected PTEN neddylation in breast cancer tissues using a

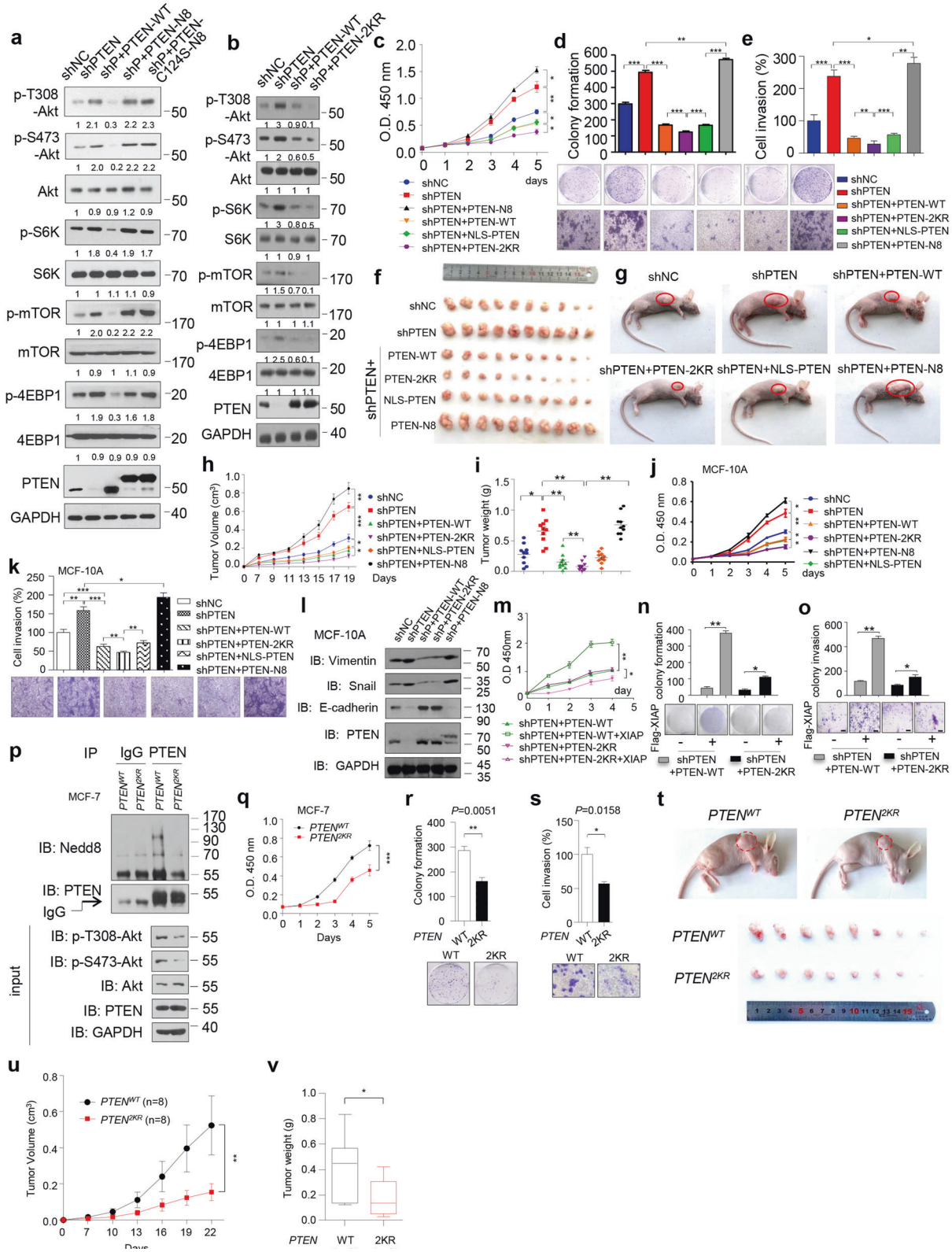

specific antibody against neddylated PTEN on K402. An analysis in a large-scale array of clinical breast cancer tissues demonstrated that the levels of neddylated PTEN were significantly increased in cancer tissues compared with adjacent normal tissues (Fig. 8a, b) and that neddylated PTEN was mainly localized to the nucleus (Fig. 8c). We further verified the relevance of PTEN neddylation to the stage of tumor development. In general, the levels of neddylated PTEN were lower in adjacent nontumor tissues and higher in tumor tissues, and there was no significant difference among different TNM stages (Fig. 8d–g). Additionally, we evaluated the possible correlation of PTEN neddylation by stratifying patients into four groups based on the cancer subtype

Fig. 5 PTEN neddylation promotes tumorigenesis. a, **b** Immunoblot of WCL from shNC, shPTEN, shPTEN-resistant PTEN-WT, PTEN-2KR PTEN-Nedd8 and PTEN-C124S-Nedd8 stable MCF-7 cells. **c**–**e** CCK8 assay (**c**), colony formation assay (**d**), and cell migration assay (**e**) were performed in the indicated cells. Data are presented as means ± SD. Results are from a representative experiment performed in triplicate. Image J was used to perform quantitative analysis. **f**–**i** Nude mice were injected subcutaneously for each of the indicated stable cell lines. The transplanted tumors were removed and photographed (**f**, **g**). Tumors were isolated, volume (**h**) and their weights were measured (**i**). Data are shown as means ± SD. **j**, **k** shNC, shPTEN, shPTEN-resistant PTEN-WT, 2KR, NLS-PTEN, PTEN-Nedd8 stable cell lines were generated in MCF-10A cells. CCK8 assay (**j**), cell migration assay (**k**), were performed in the indicated cells. **l** Immunoblot of WCL from indicated cells. **m**–**o** Flag-XIAP was stably expressed in shPTEN-resistant PTEN WT and 2KR cells. CCK8 assay (**m**), colony formation (**n**), cell migration assay (**o**), were performed in the indicated cells. Image J was used to perform quantitative analysis. **p** Immunoblot analysis of anti-PTEN immunoprecipitate and WCL from $PTEN^{WT}$ and $PTEN^{2KR}$ KI MCF-7 cells. **q**–**s** CCK8 assay (**q**), colony formation assay (**r**), cell migration assay (**s**) were performed in the indicated cells. Image J was used to perform quantitative analysis. **t**–**v** Nude mice were injected subcutaneously for each of the indicated cells. The transplanted tumors were removed and photographed (**t**). Tumors were isolated, volume (**u**) and their weights were measured (**v**). Data are shown as means ± SD. *P* values were calculated by Student's *t*-test (**r**, **s**, **v**), one-way ANOVA test (**d**, **e**, **i**, **k**, **n**, **o**) and two-way ANOVA test (**c**, **h**, **j**, **m**, **q**, **u**). $*P < 0.05$, $**P < 0.01$, $***P < 0.001$.

(luminal A/B, HER2-enriched, TNBC/basal).[55] The data showed that the levels of neddylated PTEN were higher in all of the subtypes of breast cancer than in the corresponding adjacent normal tissues (Supplementary information, Fig. S9c). Importantly, the prognostic role of PTEN neddylation in breast tumor tissues was analyzed. Patients with relatively high levels of neddylated PTEN showed poorer overall survival than those with low levels of neddylated PTEN (Fig. 8h). A high level of neddylated PTEN was also detected in breast cancer tissues (Fig. 8i). Collectively, the results suggest that breast cancer progression is accompanied by PTEN neddylation, which might be a potential prognostic marker in breast cancer.

Positive correlation of PTEN neddylation with UBA3, XIAP and FASN in cancer

Deletion of *UBA3, Ubc12*, or *XIAP* decreased the activity of the PI3K/Akt pathway in MCF-7 cells (Fig. 9a) and significantly reduced cell proliferation, colony formation and invasion (Fig. 9b–e). By contrast, knockdown of *NEDP1* showed the opposite effect. Ectopic expression of UBA3 notably increased cell proliferation and invasion (Supplementary information, Fig. S10a–c). Next, we analyzed the expression of neddylation enzymes in human breast cancer and the correlation of their expression with PTEN neddylation. Then, an analysis of a large-scale array of clinical breast cancer samples demonstrated that UBA3 and XIAP expression was significantly upregulated in breast cancer tissues compared with matched adjacent tissues (Fig. 9f, g), and NEDP1 was inversely downregulated in cancer tissues (Fig. 9h). Similar results were obtained in the analysis of tumor size (Supplementary information, Fig. S10d–f). Furthermore, the protein levels of UBA3 and XIAP were lower in low TNM stage tumors and higher in high TNM stage tumors (Fig. 9i, j; Supplementary information, Fig. S10g, h), whereas the protein levels of NEDP1 showed the opposite trend (Fig. 9k; Supplementary information, Fig. S10i). No significant difference was noted among the four subtypes (Supplementary information, Fig. S10j–l). Patients with relatively high levels of UBA3 or XIAP showed poorer overall survival, and, conversely, patients with high levels of NEDP1 showed better overall survival (Fig. 9l). By comparison, the levels among UBA3, XIAP and neddylated PTEN were positively correlated (Fig. 9m, n), while NEDP1 was negatively correlated with neddylated PTEN (Fig. 9o). In addition, we found that the relative UBA3 protein level was positively correlated with the relative XIAP protein level in breast cancer patients (Supplementary information, Fig. S10m). UBA3 was correlated with the process of tumor growth in MMTV-*PyMT* mice (Supplementary information, Fig. S10n), and the results of an integrated prognostic analysis showed that the patients with high levels of neddylated PTEN, XIAP, and UBA3 and low levels of NEDP1 displayed significantly poorer survival than did the patients with low levels of neddylated PTEN, XIAP, and UBA3 and high levels of NEDP1 (Fig. 9p). This four-molecule panel exhibited stronger predictive power than its individual constituents (Fig. 9q, r). These data suggest that the four-molecule panel might be utilized to better predict long-term prognosis in breast cancer patients.

To illustrate the correlation of nuclear neddylated PTEN levels with total PTEN, FASN, UBA3, and XIAP levels in human cancer tissues, we performed multicolor fluorescence immunohistochemistry in a breast cancer microarray. The results revealed that neddylated PTEN, UBA3, XIAP and FASN were highly expressed in breast cancer tissues (Fig. 10a–e). Although total PTEN protein expression was decreased in breast cancer patients (Fig. 10f), the levels of neddylated PTEN in the nucleus were higher in cancer tissues than in adjacent normal tissues (Fig. 10g). Neddylated PTEN levels were positively correlated with UBA3 and XIAP expression (Fig. 10h, i), and high FASN expression was positively correlated with nuclear neddylated PTEN in breast cancer patients (Fig. 10j–l). In addition, the subcellular colocalization of neddylated PTEN with total PTEN, FASN, UBA3, and XIAP was higher in breast cancer than in adjacent tissues (Fig. 10m). Collectively, these results indicate that the neddylation pathway is upregulated in breast cancer, concomitant with an enrichment of neddylated PTEN in the nucleus and high levels of FASN protein expression to promote tumor progression.

DISCUSSION

Post-translational modifications control PTEN membrane recruitment, subcellular localization, dual-phosphatase activity and protein–protein interactions. To date, ubiquitination,[14,15] SUMOylation,[16] and phosphorylation[56,57] have been shown to contribute to the translocation of PTEN and affect its tumor suppressor function. However, PTEN loss-of-function in tumorigenesis is still poorly understood. In this study, we define neddylation as a novel modification of PTEN and a critical regulatory mechanism for the loss of the tumor-suppressive function of PTEN (Fig. 10n). Nedd8 harbors the highest homology with ubiquitin among the ubiquitin-like protein family, and neddylation plays an essential role in the development of organs and progression of diseases, including cancer. Identification of genuine neddylation substrates is required to better understand the underlying mechanisms of neddylation. Eight criteria have been proposed for the characterization of Nedd8 substrates.[18] Here, we provide a series of data to prove that PTEN is a neddylation substrate. (i) Nedd8 is covalently attached to PTEN in vivo. (ii) PTEN neddylation is detectable under endogenous conditions. (iii) PTEN neddylation depends on an activating enzyme (E1, UBA3) and a conjugating enzyme (E2, Ubc12). (iv) We determined that K197 and K402 are the neddylation residues. (v) We identified XIAP as a specific ligase for PTEN neddylation both in vivo and in vitro. (vi) We identified NEDP1 as a deneddylase for PTEN. (vii) Nedd8 forms a poly-neddylation chain on PTEN. (viii) Neddylation promotes PTEN nuclear import. Collectively, based on these lines of evidence, we conclude that PTEN is a genuine neddylation substrate. To the best of our knowledge, this is the first report of PTEN neddylation.

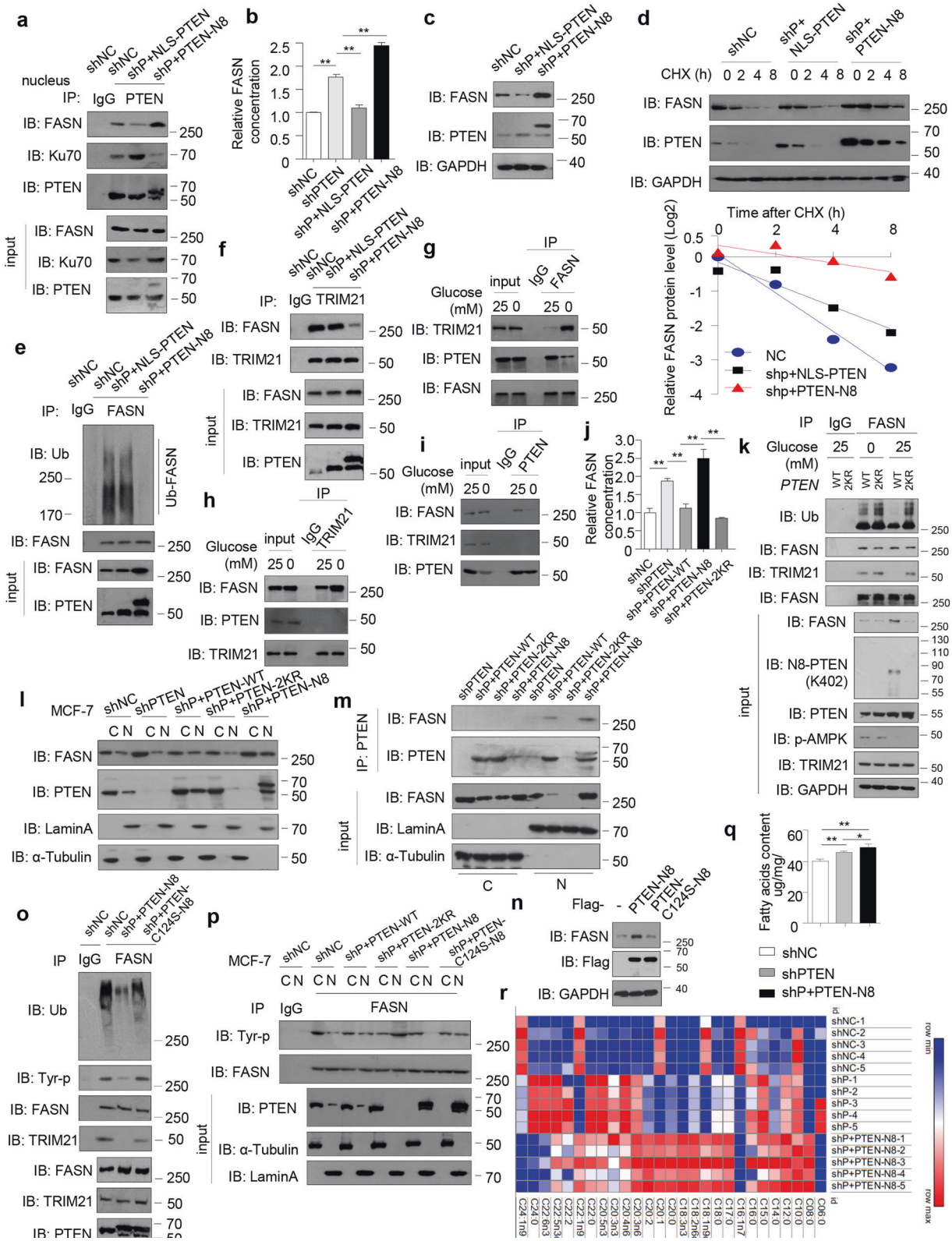

More importantly, we reveal that physiological PTEN neddylation is influenced by glucose availability. Lowering the glucose level led to a clear decrease in PTEN neddylation, while abundant levels of glucose induced PTEN neddylation. Under pathologically high glucose conditions in vivo, PTEN neddylation shows a stronger effect on tumorigenesis. Although the comprehensive mechanism still needs investigation, upregulated levels of *UBA3* and *Ubc12* mRNA were observed upon treatment with high concentrations of glucose. Thus, high levels of glucose might promote the neddylation of various substrates (not limited to PTEN), and further investigation is needed to address this. Interestingly, PTEN neddylation seems to specifically occur upon

Fig. 6 PTEN neddylation increases the stability of FASN. a Immunoblot analysis of anti-PTEN immunoprecipitate from the nuclear fractionation of shNC, shPTEN-resistant NLS-PTEN-WT and PTEN-Nedd8 stable MCF-7 cells. **b** Activity of FASN was determined by ELISA. Data represent means ± SD. $n = 3$, $^{**}P < 0.01$. **c**, **d** Immunoblot of FASN and PTEN in indicated cells, without (**c**) or with CHX (10 μM) treatment (**d**). FASN protein abundance was quantified by Image J. **e** Immunoblot analysis of anti-FASN immunoprecipitate and WCL from indicated cells. **f** PTEN-Nedd8 interferes the interaction of FASN and TRIM21. Endogenous TRIM21 protein was immunoprecipitated from the indicated cells and then detected by western blotting. **g**–**i** A trip-complex co-immunoprecipitation assay was performed. Immunoblot analysis of anti-FASN (**g**), anti-TRIM21 (**h**), or anti-PTEN (**i**) immunoprecipitate and WCL from indicated cells. **j** Activity of FASN was determined by ELISA. Data represent means ± SD. $n = 3$, $^{**}P < 0.01$. **k** Immunoblot of anti-FASN immunoprecipitate and WCL from $PTEN^{WT}$ or $PTEN^{2KR}$ MCF-7 cells. Glucose was removed and then retreated with the indicated concentration. **l** Immunoblot of FASN and PTEN from nuclear and cytoplasmic fractionation of indicated cells. **m** Immunoblot of anti-PTEN immunoprecipitate from nuclear and cytoplasmic fractionation of indicated cells. **n** Immunoblot of FASN from MCF-7 cells transfected with Flag-PTEN-Nedd8 or Flag-PTEN C124S-Nedd8. **o** Immunoblot of anti-FASN immunoprecipitate and WCL from indicated cells. **p** Nuclear and cytoplasmic fractions were generated and immunopurified with antibodies against FASN. The immunoprecipitate and WCL were analyzed by western blotting. **q**, **r** Lipid metabolism was detected by GC-FID/MS in shNC, shPTEN, shPTEN-resistant PTEN-Nedd8 stable cell lines. Total free fatty acids (FFA) levels were analyzed (**q**). Heatmap was performed and the significant differences were analyzed using Student's *t*-test, $n = 5$ (**r**). Cell-based studies were repeated at least three times independently. Data present means ± SD. *P* values were calculated by both one-way ANOVA test (**b**, **j**, **q**) and two-way ANOVA test (**d**). ns, not significant, $^{*}P < 0.05$, $^{**}P < 0.01$, $^{***}P < 0.001$.

glucose stimulation since neither genotoxic stress (DNA damage) nor oxidative stress had a significant effect on PTEN neddylation. Previous studies showed that PTEN SUMOylation and phosphorylation occur in response to genotoxic stress and oxidative stress, respectively, and both modifications contribute to nuclear-cytoplasmic regulation. Interestingly, glucose-induced nuclear translocation of PTEN might be dependent on neddylation. Deletion of *UBA3*, *Ubc12* or *XIAP* inhibited glucose-induced nuclear import of PTEN, and mutating the neddylation lysines on PTEN to arginines blocked the nuclear import of PTEN upon glucose stimulation. Here, neddylation shows the potential for dynamic regulation of PTEN compartmentalization in response to glucose uptake or deprivation. It is noteworthy that high levels of glucose govern $PTEN^{K27\text{-}polyUb}$ and switch PTEN phosphatase activity to direct epithelial–mesenchymal transition.[25] Therefore, glucose attempts to regulate the tumor-suppressive function of PTEN in multiple ways, and more investigations are required in the future. Previous studies have indicated that neddylation plays a key role in certain nuclear processes.[37,44,45] Here, we found that Nedd8 interacts with several nuclear pore-targeting proteins, which may provide a potential mechanism by which neddylation promotes the nuclear import of substrates. Nucleus–cytoplasm transport is a complex process dependent on importin and exportin proteins, as well as the small GTPase Ran. Therefore, more evidence is needed to support this point in future studies. Additionally, it is worth noting that the K402 site has been proven to be acetylated by CBP.[48] However, in contrast to neddylation, our findings suggest that acetylation on K402 does not influence PTEN localization. Acetylation of PTEN at the K402 site preferentially occurs at low glucose concentrations, but PTEN neddylation requires high glucose concentrations. Importantly, endogenous PTEN neddylation was detectable when breast tumors began to spontaneously develop in MMTV-*PyMT* mice, and the level of modified PTEN increased gradually and was accompanied by tumor progression. Depletion of *NEDP1* in MMTV-*PyMT* mice further shortened the tumor-forming time in conjunction with elevated levels of neddylated PTEN and excessive activity of the PI3K/Akt signaling pathway. These results suggest that PTEN neddylation is a natural molecular event during tumor development.

Surprisingly, we found that nuclear neddylated PTEN acts as a tumor-promoting protein rather than tumor-suppressing protein. In the last decade, the function and regulation of nuclear PTEN have attracted increasing attention, and nuclear PTEN proteins have been widely recognized to suppress tumorigenesis through multiple mechanisms, including the maintenance of chromosome integrity.[49–51] In agreement with earlier studies, our data confirmed that NLS-PTEN exerts a predominantly tumor-suppressive function. However, neddylated PTEN (linking Nedd8 to the C-terminus of PTEN to mimic neddylated PTEN) in the nucleus intends to induce tumorigenicity. By contrast, unneddylatable PTEN ($PTEN^{2KR}$ KI) showed stronger tumor-suppressive activity than did WT PTEN. Therefore, we now demonstrate a striking finding and evidence for two distinct pools of nuclear PTEN, i.e., neddylated and unneddylated PTEN, each with an opposing effect on oncogenesis. Unneddylated PTEN functions as a tumor suppressor, whereas neddylated PTEN functions as a tumor promoter.

Regarding the mechanism of the tumor-promoting role of nuclear PTEN modified by Nedd8, we show that neddylation promotes the nuclear localization of PTEN. Such translocation reduces the inhibitory effects of PTEN on the PI3K/Akt signaling pathway. Recently, increasing evidence also supports the concept that neddylation enhances Akt signaling in cancer.[58,59] On the other hand, neddylated PTEN appears to gain an oncogenetic function in the nucleus. We identified that neddylated PTEN interacted with FASN in the nucleus; FASN is a key lipogenic enzyme, and increased FASN activity leads to elevated de novo fatty acid synthesis to support tumorigenesis.[52] FASN has been considered a potential and druggable target for the chemoprevention of breast cancer.[60,61] TRIM21 has been identified as a polyubiquitination E3 ligase for FASN.[53] Nuclear neddylated PTEN dephosphorylated FASN in the nucleus, which prevents TRIM21 from interacting with FASN to influence its protein stability. Consequently, FASN-mediated de novo fatty acid synthesis is elevated. These results indicate a novel explanation of how neddylation induces tumor progression.

We demonstrate that PTEN neddylation positively contributes to the progression of breast cancer and correlates with poor prognosis. Although total PTEN protein levels were decreased in breast cancer patients, the levels of neddylated PTEN in the nucleus were higher in cancer tissues than in matched adjacent tissues. Neddylated PTEN is positively correlated with UBA3, XIAP and FASN, and high levels of FASN expression were positively correlated with nuclear neddylated PTEN in breast cancer patients. The role of PTEN neddylation in additional types of human cancers needs further investigation, and it is also worth exploring the proportion and predominant role of neddylated and unneddylated PTEN in human tumorigenesis.

Taken together, the data in this work define neddylation as a critical modification of PTEN and reveal a previously unidentified tumor-promoting role of nuclear PTEN, which is covalently conjugated with Nedd8. Our findings open up avenues for precision cancer therapies that target neddylated proteins.

MATERIALS AND METHODS

Mouse and reagents

The $NEDP1^{-/-}$ mice were generated by Nanjing Biomedical Research Institute of Nanjing University. A loxP floxed neo cassette was inserted in frame into the *NEDP1* gene to generate the targeting vector. All mice were maintained and handled in accordance with protocols approved by the Beijing Institute of Lifeomics. Routine

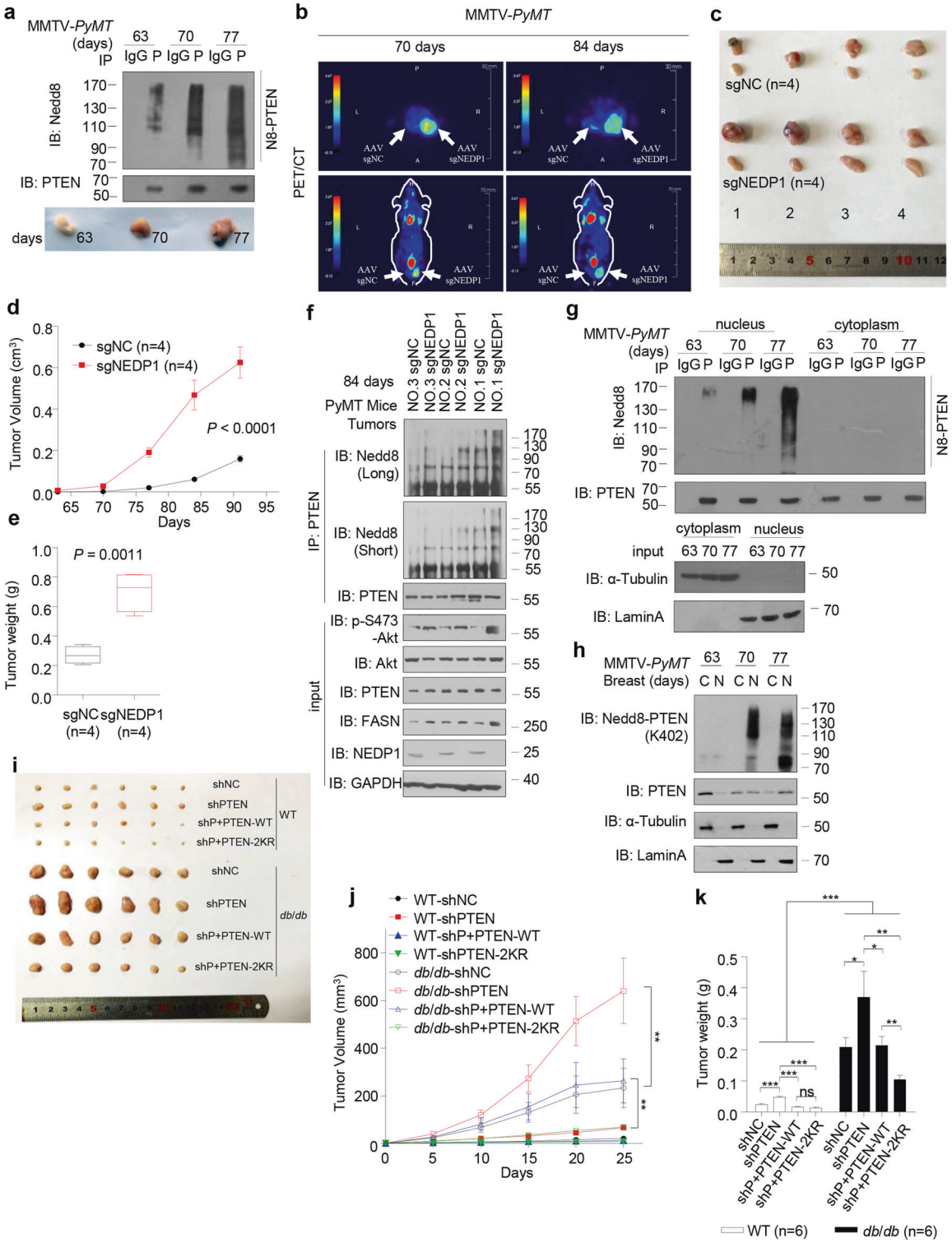

genotyping primers were listed in Supplementary information, Table S1. MMTV-*PyMT* mice (*PyMT*/WT mice, FVB/N background) were kindly gifted by Professor Mingyao Liu from East China Normal University. The *db/db* mice were purchased from Shanghai Model Organisms Center, Inc. The NAE inhibitor MLN4924 (HY-70062), proteasome inhibitor MG132 (HY-13259), XIAP inhibitor Embelin (HY-17473), p300/CBP inhibitor ICBP112 (HY-19541), 2-Deoxy-D-glucose (a glucose analog and a competitive inhibitor of glucose metabolism) (2-DG, HY-13966) were purchased from MCE. Cisplatin (P4394) and methyl methane sulfonate (MMS) (129925) were purchased from Sigma Aldrich. SUMOylation inhibitor 2-D08 (S8696) was purchased from Selleck. The antibody details were listed in Supplementary information, Table S2.

Cell culture and transfections

MCF-7, MDA-MB-231, MDA-MB-468, 4T1, HEK293T cell lines were purchased from ATCC, and authenticated by STR profiling and tested for mycoplasma contamination by GENEWIZ. MCF-10A (a

Fig. 7 PTEN neddylation promotes MMTV-*PyMT* mice more prone to tumorigenesis. a Immunoblot analysis of anti-PTEN immunoprecipitate from spontaneous breast tumors of MMTV-*PyMT* mice. Data of three mice measured through 63–77 days of age are shown. **b**–**e** *NEDP1* knockout increased the uptake of ^{18}F-FDG in breast tumors of MMTV-*PyMT* mice. AAV-sgNC and AAV-sgNEDP1 were injected in the lower left and lower right side of mammary fat pads of MMTV-*PyMT* mice at 56 days, respectively. Representative whole-body images of *PyMT* littermates with breast tumors were obtained from micro-PET/CT imaging after 14 and 28 days of AAV injections. ^{18}F-FDG uptake was analyzed 1 h after injection. White arrows point to tumor (**b**). The tumors were removed and photographed (**c**). Tumors were isolated, volume (**d**) and weights (**e**) were measured. Data are shown as means ± SD. **f** Immunoblot analysis of anti-PTEN immunoprecipitate from spontaneous breast tumors of MMTV-*PyMT* mice injected with AAV-sgNC or AAV-sgNEDP1. **g**, **h** Nuclear PTEN was neddylated in MMTV-*PyMT* mice. Immunoblot analysis of anti-PTEN immunoprecipitate from nuclear and cytoplasmic fractionation of MMTV-*PyMT* spontaneous breast tumors (**g**). Immunoblot of neddylated PTEN on K402 (**h**). **i**–**k** Diabetic *db/db* and control mice were injected subcutaneously for each of the indicated 4T1 stable cell lines. The transplanted tumors were removed and photographed (**i**). Tumors were isolated, volume (**j**) and weights (**k**) were measured. Data are shown as means ± SD. *P* values were calculated by Student's *t*-test (**e**), one-way ANOVA test (**k**) and two-way ANOVA test (**d**, **j**). ns, not significant, $^{*}P < 0.05$, $^{**}P < 0.01$, $^{***}P < 0.001$.

human non-tumorigenic breast epithelial cell line) cells were kindly gifted by Qinong Ye from Beijing Institute of Biotechnology. HEK293T *NEDP1*$^{+/+}$ and *NEDP1*$^{-/-}$ cells were kindly gifted by Professor Xiaofeng Zheng from Peking University. MCF-7, MDB-MA-468, HEK293T, HEK293T *NEDP1*$^{+/+}$ and *NEDP1*$^{-/-}$ cells were cultured in DMEM medium supplemented with 10% fetal bovine serum (FBS). MDA-MB-231 cells were cultured in Leibovit's L-15 medium supplemented with 10% FBS. MCF-10A cells were cultured in mammary epithelial cell growth medium (Promo Cell, C-39115) with 10% horse serum, New Zealand Origin (Invitrogen, 16050-114). Mouse 4T1 cells were cultured with MEM medium supplemented with 10% FBS. Cells were transfected with various plasmids using TuboFect (Thermo Fisher Scientific, R0531), Sage LipoPlus^{TM}, Lipofectamine 3000 (Invitrogen, L3000001) according to the manufacturer's protocol.

Immunoprecipitation and immunoblotting

For immunoprecipitation assays, cells were lysed in EBC lysis buffer (0.5% NP-40, 50 mM Tris, pH 7.6, 120 mM NaCl, 1 mM EDTA, 1 mM Na_3VO_4, 50 mM NaF and 1 mM β-mercaptoethanol) supplemented with protease inhibitor cocktail (Roche, 11836170001). Immunoprecipitations were performed using the indicated primary antibody and protein A/G agarose beads (Santa Cruz, sc-2003) at 4 °C. The immunoprecipitants were washed at least three times in NETN lysis buffer (150 mM NaCl, 1 mM EDTA, 50 mM Tris-HCl, pH7.8, 1% NP-40, 1 mM phenylmethylsulfonyl fluoride) before being resolved by SDS-PAGE and immunoblotted with indicated antibodies.

RNA interference

siRNAs against *Mdm2* (sc-29394), *Roc1* (sc-44072), *c-Cbl* (sc-29242), *XIAP* (sc-37508), *Nedd4-1* (sc-41079), *WWP2* (sc-40362), *WWP1* (sc-40366), *NEDP1* (sc-44452) were purchased from Santa Cruz Biotechnology. Sequence information of the siRNA, shRNA and sgRNA is provided in Supplementary information, Table S3.

In vivo modification assays

Cells were solubilized in modified lysis buffer (50 mM Tris, pH 7.4, 150 mM NaCl, 10% glycerol, 1 mM EDTA, 1 mM EGTA, 1% SDS, 1 mM Na_3VO_4, 1 mM DTT and 10 mM NaF) supplemented with a protease inhibitor cocktail. The cell lysate was incubated at 60 °C for 10 min. The lysate was then diluted 10 times with modified lysis buffer without SDS and incubated with the indicated antibody for 3 h at 4 °C before adding Protein A/G-plus Agarose (Santa Cruz, sc-2003). Then the lysate was rotated gently for 8 h at 4 °C. The immunoprecipitants were washed at least three times in wash buffer (50 mM Tris, pH7.4, 150 mM NaCl, 10% glycerol, 1 mM EDTA, 1 mM EGTA, 0.1% SDS, 1 mM DTT and 10 mM NaF). Proteins were analyzed by western blotting with indicated antibodies.

In vitro modification assays

GST-PTEN and His-XIAP were expressed in *Escherichia coli* BL21 (DE3). For the Neddylation assay, 0.5 μg of GST-PTEN, 0.5 μg of His-XIAP were incubated with 2 μg of Nedd8, 10 ng of E1 (APPBP1-UBA3) and 200 ng of E2 (Ubc12) in a total reaction volume of 20 μL Nedd8 conjugation Rxn Buffer Kit (BostonBiochem, SK-20). Nedd8 (UL-812), Nedd8 E1 (APPBP1/UBA3) (E-313), Ubc12 (A-655) were purchased from BostonBiochem. Samples were incubated at 30 °C for 1 h, and reactions were terminated with SDS-PAGE loading buffer before western blotting.

His pull-down by Ni-NTA columns

Cells were collected and resuspended in binding buffer (6 M guanidine HCl, 0.1 M Na_2HPO_4, 0.1 M NaH_2PO_4, 0.01 M Tris (pH8.0), 10 mM β-mercaptoethanol, 5 mM NEM, 5 mM imidazole) and incubated with Ni^{2+}-NTA Superflow Cartridges (QIAGEN, 17-5318-02) at 4 °C for 12 h. Immunoblotting was performed using indicated antibodies.

Generation of knockout cells

The knockout cell lines were generated using the CRISPR–Cas9 method. CRISPR guide sequences targeting *PTEN*, *UBA3*, *Ubc12*, *XIAP* and *NEDP1* were designed by software at http://crispr.mit.edu and cloned into lenti-Crispr pXPR_001. The sgRNA sequences were listed in Supplementary information, Table S3. MCF-7 and MCF-10A cells were co-transfected with the Lenti-Crispr vector and packaging plasmids pVSVg and psPAX2. Puromycin-resistant single cells were plated in a 96-well dish to screen for positive monoclonal cells.

Fluorescence microscopy

After fixation with 4% paraformaldehyde and permeabilization in 0.2% Triton X-100 (PBS), cells were incubated with the indicated antibodies for 12 h at 4 °C, followed by incubation with goat anti-rabbit IgG H&L Alexa Fluor 488 or 594 antibody for 1 h at 37 °C. The nuclei were stained with DAPI, and images were visualized with a Zeiss LSM 510 Meta inverted confocal microscope.

Cell fractionation

Nuclear fractions were prepared by using the Minute TM Nuclear and Cytoplasmic Extraction Reagents Kit (Invent biotech, SC-003) according to the manufacturer's protocol.

Real-time PCR

Total RNA was isolated and converted to cDNA using the ReverTra Ace® (Toyobo, TRT-101). Quantitative PCR reactions were carried out using SYBR Green PCR master mix (Toyobo, QPK201). Primers were shown in Supplementary information, Table S4.

Cell proliferation assay

Cells were plated on 96-well plates (1000 cells per well). After adding Cell Counting Kit-8 (Dojindo, CK04) to the wells for 1 h, cell numbers were measured at 450 nm. Each cell line was set up in 4 replicate wells, and the experiment was repeated three times.

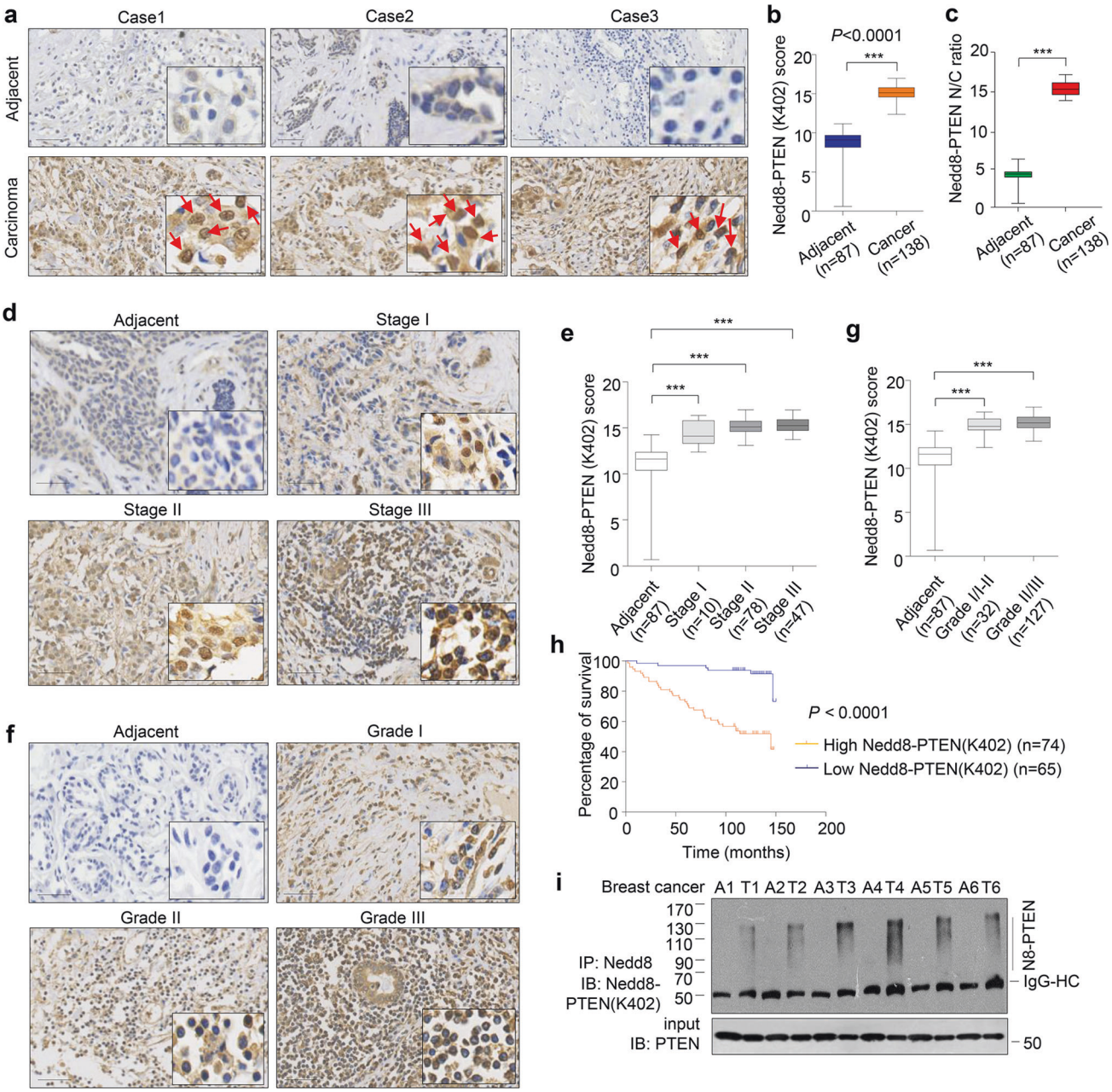

Fig. 8 PTEN neddylation is elevated in breast cancer patients. a Representative image from immunohistochemical staining of PTEN neddylation on K402 in tumors and matched adjacent tissue from three cases in different pathological grades. Image J was used to perform Semi-quantitative analysis. Scale bars, 50 μm. **b** PTEN neddylation on K402 expression scores are shown as box plots. Data were analyzed using the Kruskal-Wallis test. **c** PTEN immunoreactivity in cytoplasm (C) and nucleus (N) were semi-quantitatively analyzed by NIH Image J 1.62 software. PTEN N/C ratio expression scores are shown as box plots. **d**, **f** Representative images from immunohistochemical staining of neddylated PTEN on K402 in two serial sections of the same tumor in different stages (**d**) and grades (**f**) are shown. Scale bars, 50 μm. **e**, **g** Box plot of PTEN neddylation on K402 in tumors with different stages (**e**) and grades (**g**). Data were analyzed using the Kruskal-Wallis test. Image J was used to perform Semi-quantitative analysis. **h** Kaplan-Meier plot of overall survival of patients with breast carcinomas. A log-rank test was used to show differences between groups. **i** PTEN neddylation was higher in breast tumor patients. Immunoblot analysis of anti-PTEN immunoprecipitate from adjacent and breast cancer tissues. A, adjacent tissue; T, tumor tissue. *P* values were calculated by Student's *t*-test (**b**, **c**), one-way ANOVA test (**e**, **g**) and log-rank test (**h**). ***$P < 0.001$.

Colony formation assay

Cells were seeded into 6-well tissue culture plate with 6000 cells per well. Plates were incubated at 37 °C and 5% CO_2 and colonies were scored 21 days after preparation.

Cell migration assay

The assay was performed in an invasion chamber consisting of a 24-well tissue culture plate with 12 cell culture inserts (Becton-Dickinson). A cell suspension in serum-free culture medium (5×10^4 cells per well) was added to the inserts, and each insert was placed in the lower chamber containing 10% FBS culture medium. Cells were allowed to migrate for 24 h in a humidified chamber at 37 °C with 5% CO_2. Then filter was removed and fixed with 4% formaldehyde for 20 min. Cells located in the lower filter were stained with 0.1% crystal violet for 15 min and photographed.

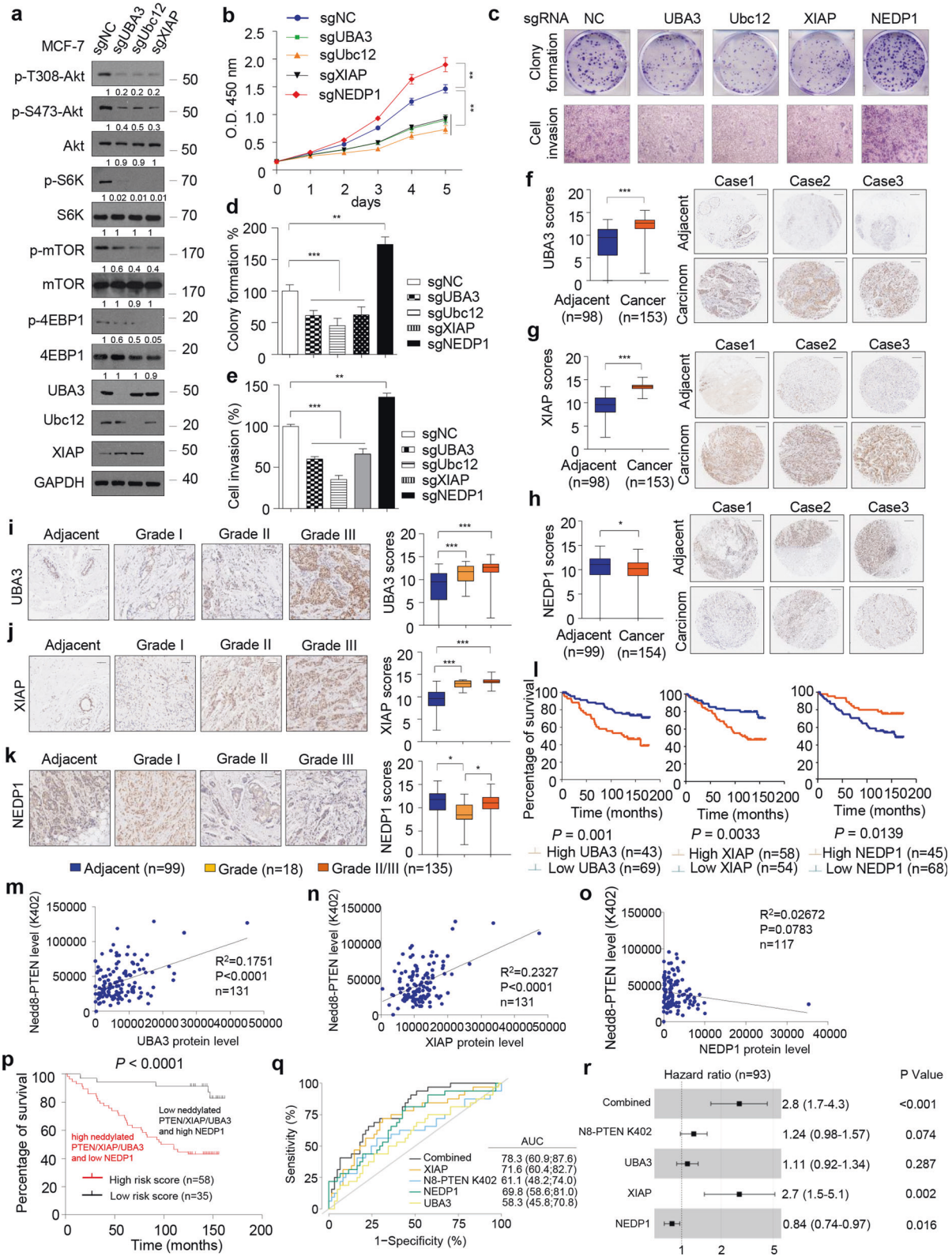

Tumor growth in mice

The experimental procedures in mice have been approved by the Animal Care and Use Committee of Academy of Military and Medical Sciences. BALB/c nude mice (6-week old, 18.0 ± 2.0 g) were obtained from Shanghai Laboratory Animal Center (SLAC, China). Diabetic *db/db* mice (6-week old, 35 ± 2 g) were obtained from Shanghai Model Organisms Center, Inc. (SMOC, China). Cells (5×10^6 per mouse) were inoculated subcutaneously into the right flank of the mice. Tumor size was measured every 3 days and converted to TV according to the following formula: TV (mm^3) = $(a \times b^2)/2$, where a and b are the largest and smallest diameters, respectively. All animals were killed 4 weeks after injection, and the transplanted tumors were removed, weighed and fixed.

Fig. 9 Positive correlation of PTEN neddylation with neddylation enzymes in breast cancer. a Deletion of *UBA3*, *Ubc12* and *XIAP* attenuated PI3K/Akt activation. Immunoblot of WCL from *UBA3*-, *Ubc12*- and *XIAP*-deleted MCF-7 cells. **b**–**e** UBA3, Ubc12 and XIAP promoted tumorigenesis, while NEDP1 was in the opposite. CCK8 assay (**b**), colony formation assay (**c**, **d**), and cell invasion assay (**e**) were performed in indicated cells. Data are presented as means ± SD. Results are from a representative experiment performed in triplicate. Image J was used to perform semi-quantitative analysis. **f**–**h** Representative images from immunohistochemical staining of UBA3 (**f**), XIAP (**g**) and NEDP1 (**h**) in tumors and matched adjacent tissue. The expression scores are shown as box plots. Scale bars, 250 μm. Image J was used to perform semi-quantitative analysis. **i**–**k** Representative images from immunohistochemical staining of UBA3 (**i**), XIAP (**j**) and NEDP1 (**k**) in different grades are shown. The expression scores are shown as box plots. Scale bars, 100 μm. Data were analyzed using the Kruskal-Wallis test. Image J was used to perform semi-quantitative analysis. **l** Kaplan-Meier plot of overall survival of 112 patients with breast carcinomas (the two groups were stratified by UBA3, XIAP and NEDP1 expression level median). A log-rank test was used to show differences between groups. **m**–**o** Positive correlation of UBA3 (**m**), XIAP (**n**), or NEDP1 (**o**) with PTEN neddylation on K402 site. Data were calculated by both Chi-Square and Mann-Whitney tests. Image J was used to perform semi-quantitative analysis. **p** The Risk score was calculated as a sum of multiplication of the expression level of each protein and its respective Cox regression coefficient identified from the tissue microarray. Risk score = Σ (expression level of protein) × (Cox regression coefficient). Each Cox regression coefficient used for Risk score computation is shown as follows: neddylated PTEN on K402 = 0.214; UBA3 = 0.102; XIAP = 1.063; NEDP1 = –0.169. The two groups (High group and Low group) were divided by median of Risk score. Black and red Kaplan-Meier curves represent predicted low-risk and high-risk groups, respectively. Cox regression model and K-M survival curves were used via the survival package in R/Bioconductor. **q**, **r** Comparison of prognostic efficiencies between the four-molecule panel and its individual constituents, as well as clinicopathologic variables. The ROC curves (**q**), forest plots (**r**) of the four-molecule panel (risk score) and single markers in this cohort. *P* values were calculated by Student's *t*-test (**d**–**k**); two-way ANOVA test (**b**); Kaplan-Meier log-rank test (**l**, **p**), Pearson correlation test (**m**, **n**, **o**) and Cox regression test (**r**). $^{*}P < 0.05$, $^{**}P < 0.01$, $^{***}P < 0.001$.

Cohort and immunohistochemistry

The breast tissue microarrays were purchased from Shanghai Biochip Company (HBre-Duc170Sur-01, HBre-Duc139Sur-01, HBre-Duc090Sur-01) and Shanghai Superbiotek Company (BRC1601). HBre-Duc170Sur-01 and HBre-Duc090Sur-01 were immunostained with NEDP1, UBA3 and PTEN (Supplementary information, Data S4 and S6). HBre-Duc139Sur-01 and HBre-Duc090Sur-01 were immunostained with Nedd8-PTEN K402 antibody (Supplementary information, Data S5). The patient's pathological information in HBre-Duc139Sur-01 is fully included in the HBre-Duc170Sur-01 array. Breast cancer tumors and matched adjacent normal tissues were approved by the department of breast and thyroid Surgery at the Second People's Hospital of Shenzhen (14 cases in Supplementary information, Data S7). BRC1601 were used for multicolor fluorescence immunohistochemistry with neddylated PTEN on K402, FASN, UBA3, XIAP and PTEN antibodies (Supplementary information, Data S8). All staining was assessed by a quantitative imaging method; the percentage of immunostaining and the staining intensity were recorded. An H-score was calculated using the following formula: H-score = Σ (PI × I) = (percentage of cells of weak intensity × 1) + (percentage of cells of moderate intensity × 2) + (percentage of cells of strong intensity × 3). PI indicates the percentage of positive cells versus all cells.

ELISA assay

The quantitation of FASN level was performed using ELISA assay kit (Biomatik, EKU04054) according to the manufacturer's instructions.

LC-MS/MS analysis

Proteins in IP samples were precipitated with IP buffer (0.5% NP-40, 50 mM Tris, pH 7.6, 120 mM NaCl, 1 mM EDTA, 1 mM Na_3VO_4, 50 mM NaF and 1 mM b-mercaptoethanol) and then washed three times with IP buffer. The samples from in-gel digestion were analyzed on a Thermo™ Q Exactive (Thermo Fisher Scientific) interfaced with an EASY-nLC 1000 UPLC system (Thermo Fisher Scientific). The tryptic peptides were dissolved in 0.1% FA, directly loaded onto a reversed-phase precolumn (Acclaim PepMap 100, Thermo). Peptide separation was performed using a reversed phase analytical column (Acclaim PepMap RSLC, Thermo). The gradient was comprised of an increase from 6% to 25% solvent B (0.1% FA in 98% ACN) over 16 min, 25% to 40% over 6 min and climbing to 80% in 4 min then holding at 80% for the last 4 min, all at a constant flow rate of 320 nL/min on an EASY-nLC 1000 UPLC system. The peptides were subjected to NSI source followed by tandem mass spectrometry (MS/MS) in Q Exactive™ (Thermo) coupled online to the UPLC. Intact peptides were detected in the orbitrap at a resolution of 70,000. Peptides were selected for MS/MS using NCE setting as 28; ion fragments were detected in the orbitrap at a resolution of 17,500. A data-dependent procedure that alternated between one MS scan followed by 20 MS/MS scans was applied for the top 20 precursor ions above a threshold ion count of 5E3 in the MS survey scan with 15.0 s dynamic exclusion. The electrospray voltage applied was 2.0 kV. Automatic gain control (AGC) was used to prevent overfilling of the orbitrap; 5E4 ions were accumulated for generation of MS/MS spectra. For MS scans, the m/z scan range was 350 to 1800. The resulting MS/MS data were processed using Mascot search engine (v.2.3.0). Tandem mass spectra were searched against Swissport *Human* database. Trypsin/P was specified as cleavage enzyme allowing up to 2 missing cleavages. Mass error was set to 10 ppm for precursor ions and 0.02 Da for fragment ions. Carbamidomethyl on Cys were specified as fixed modification and oxidation on Met, acetylation on Protein N-term were specified as variable modifications. Peptide ion score was set ≥ 20. Protein identification data (accession numbers, peptides observed, sequence coverage) are available in Supplementary information, Data S1 and S3, respectively. All raw data and search results have been deposited to the PRIDE database (http://www.iprox.org/index). The accession numbers are PXD011368 (Supplementary information, Data S1), PXD021544 (Supplementary information, Data S2) and PXD011395 (Supplementary information, Data S3).

GC-FID/MS analysis of fatty acids

Fatty acid composition was measured in the methylated forms. About 5 mg protein lysed from indicated cells was homogenized with 5% methanol sulfate and 0.2% BHT methanol at 90–95 °C water bath for 1.5 h. Then Saturated saline and N-hexane were added before centrifugation 5 min at 4 °C. Methyl-19-carbonate was added and vortexed for 10 s. After methylated, fatty acid composition was analyzed using 7890B Gas Chromatograph (GC) 5977 A Mass Selective Detector (MSD) (Agilent Technologies, USA) which was equipped with a flame ionization detector (FID) and a mass spectrometer carrying an electron impact (EI) ion source. An Agilent DB-225 capillary GC column (10 m, 0.1 mm ID, 0.1 μm film thickness) was used with 1 μL sample injection volume and a splitter (1:30). The temperature of injection port and detector was set at 230 °C. The column temperature was programmed with 55 °C for 1 min, and then increased to 205 °C with a rate of 30 °C per min. Column temperature was kept at 205 °C for following 3 min and increased to 230 °C at 5 °C per min. For identification, the methylated fatty acids were compared with a chromatogram from a mixture of 37 known

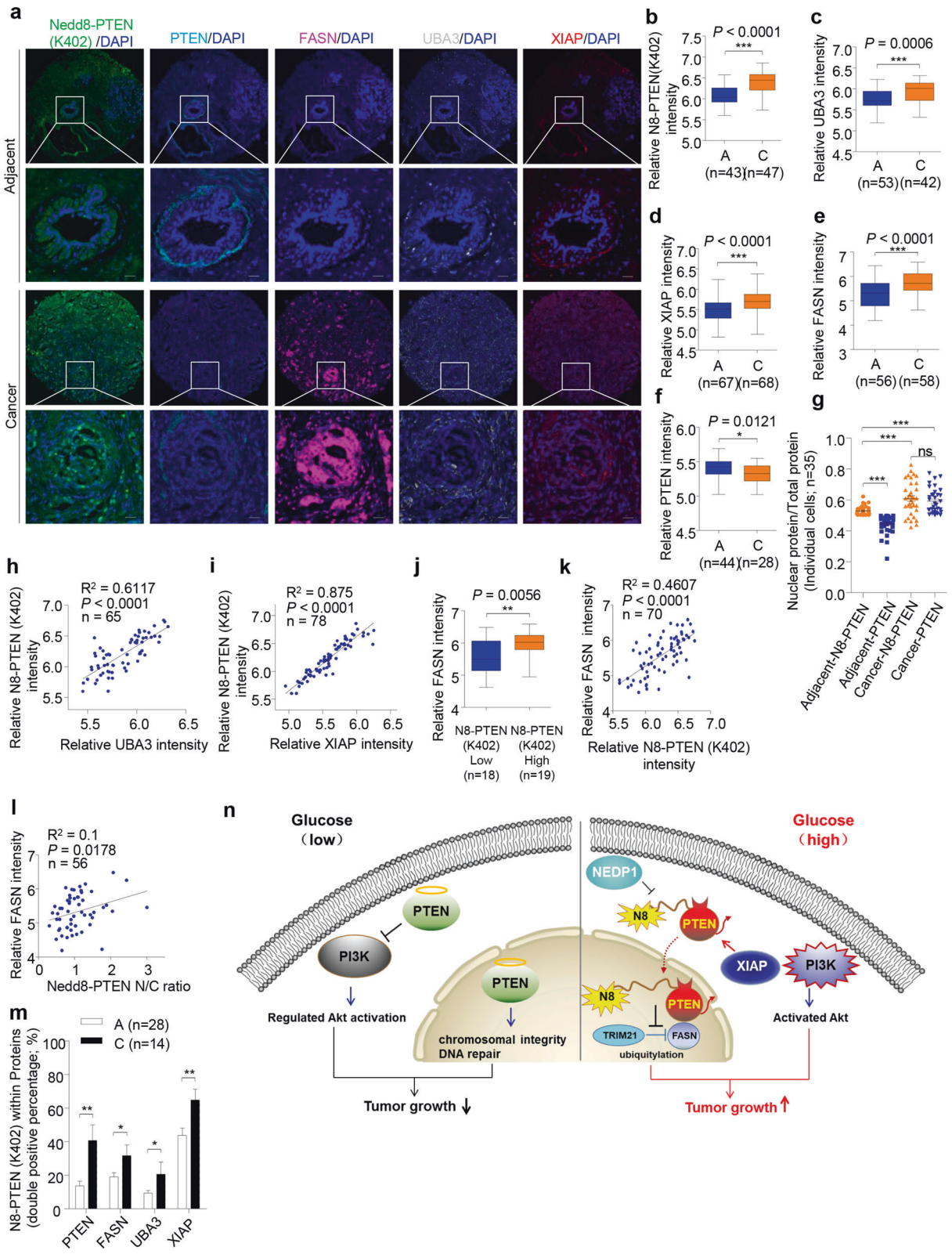

standards and then confirmed with their mass spectral data. Each fatty acid was quantified with the FID data by comparing its signal integrals with peak integrals of internal standards. These data were expressed as μmol of fatty acids per gram of tissue, which are available in Supplementary information, Data S9.

Micro-PET/CT

Before 18F-FDG administration, mice were deprived of food for 8–12 h. 18F-FDG (11.1 MBq (300 mCi) in 0.2 mL) was injected through the tail vein. Micro-PET/CT imaging was started 1 h after 18F-FDG injection. Micro-PET/CT images was performed on a

Fig. 10 The correlation of neddylated PTEN with neddylation enzymes and FASN in the progression of breast cancer. a Representative image from immunofluorescence staining of neddylated PTEN on K402, PTEN, FASN, UBA3 and XIAP in breast cancer and adjacent normal tissues. Scale bars, 40 μm. **b**–**f** Quantification of the relative intensities of neddylated PTEN on K402 (**b**), UBA3 (**c**), XIAP (**d**), FASN (**e**) and PTEN (**f**), is shown as box plots. Image J was used to perform semi-quantitative analysis. **g** The levels of PTEN or neddylated PTEN on K402 in nucleus were semi-quantitatively analyzed by inForm 3.0 software. Whisker plots show the relative nuclear/total protein ratio. **h**, **i** Positive correlation of neddylated PTEN on K402 with UBA3 (**h**) and XIAP (**i**). Image J was used to perform semi-quantitative analysis. **j** Relative intensities of FASN in breast cancer tissues with high or low level of neddylated PTEN on K402 were analyzed. **k** Positive correlation of neddylated PTEN on K402 with FASN. Image J was used to perform semi-quantitative analysis. **l** Positive correlation of PTEN nuclear (N)/cytoplasm (C) ratio with FASN. **m** Percentages of positive area of neddylated PTEN on K402 within the total positive area of indicated proteins in breast cancer tissues (C) and adjacent normal tissues (A) were analyzed. **n** A model for neddylation in regulating PTEN nuclear import and promoting tumor development. Left, in cells with low glucose concentration, PTEN functions as a potent tumor suppressor that inhibits the PI3K/Akt signaling pathway in the cytoplasm and maintains chromosomal integrity, controls DNA repair in the nucleus. Right, in cells with high glucose concentration, PTEN neddylation is catalyzed by XIAP ligase and removed by NEDP1 deneddylase. Neddylation induces PTEN nuclear import (N8 stands for Nedd8) and PI3K/Akt pathway activation. Neddylated PTEN stabilizes FASN and promotes fatty acid synthesis through interfering the interaction between FASN and the ubiquitin ligase TRIM21. Therefore, neddylated PTEN shows an unexpected tumor-promoting function. *P* values were calculated by Student's *t*-test (**b**–**f**, **j**, **m**); one-way ANOVA test (**g**) and Pearson correlation test (**h**, **i**, **k**, **l**). ns, not significant, $*P < 0.05$, $**P < 0.01$, $***P < 0.001$.

Super Nova PET/CT scanner (PINGSENG Healthcare (Kunshan) Inc.). For micro-PET/CT imaging, all mice were subjected to isoflurane anesthesia (1%–2% in 100% oxygen) on a temperature self-adjust tube to maintain body temperature throughout the procedure. Mice were visually monitored for breathing and any other signs of distress throughout the full imaging period. The images were reconstructed using a three-dimensional ordered subsets expectation maximum algorithm (OSEM) without attenuation correction. For data analysis, the region of interest (ROI) was manually drawn to cover the whole tumor on fused images.

Further information of materials and methods is listed in Supplementary information, Data S10.

Ethics statement

All animals were handled in strict accordance to the "Guide for the Care and Use of Laboratory Animals" and the "Principles for the Utilization and Care of Vertebrate Animals", and all animal work was approved by the Institutional Animal Care and Use Committee (IACUC) at the Beijing Institute of Lifeomics. The clinical samples were approved by the department of breast and thyroid surgery at the Second People's Hospital of Shenzhen. Informed consent was obtained from all subjects or their relatives.

Statistical analysis

All data were representative of no less than three independent experiments. All data were presented as means ± SD. Data were analyzed using SPSS 19.0 (IBM Corp., Armonk, NY, USA) and GraphPad Prism 5 (GraphPad Software, Inc., La Jolla, CA). The differences between groups were assessed by Student's *t*-test. The correlations were analyzed using Pearson correlation test. A value of $P < 0.05$ was considered to be statistically significant.

DATA AVAILABILITY

For IP-MS, all raw data and search results have been deposited to the PRIDE database (http://www.iprox.org/index) with the accession number: PXD011368 (Supplementary information, Data S1); PXD021544 (Supplementary information, Data S2); PXD011395 (Supplementary information, Data S3). The authors declare that all the relevant data supporting the findings of this study are available within the article and its Supplementary information files, or from the corresponding author on reasonable request.

ACKNOWLEDGEMENTS

We thank Drs. Mian Wu (University of Science and Technology of China, Anhui Province, China), Xiaofeng Zheng (Peking University, Beijing, China), Mingyao Liu (East China Normal University, Shanghai, China), Qinong Ye (Beijing Institute of Biotechnology) for kindly providing materials. This work was jointly supported by the National Key R&D Program of China (2017YFA0505602), Chinese National Basic Research Programs (2015CB910401), Chinese National Natural Science Foundation Project (31670774, 31971229), Beijing Natural Science Foundation Project (Z151100003915083), Open Project Program of the State Key Laboratory of Proteomics (SKLP-O201901), Support Project of High-level Teachers in Beijing Municipal Universities in the Period of 13th Five-year Plan (CIT&TCD201704097) and Beijing excellent talents training project.

AUTHOR CONTRIBUTIONS

The project was conceived by L.Z. The experiments were designed by L.Z., P.X. and F. H. Most of the modification experiments were performed by P.X. The cell biology function experiments were contributed by Z.P., P.X., and M.D. The animal experiments were contributed by Z.P., H.L. and X.Z. The breast cancer sample collection and immunohistochemical analysis were contributed by Z.P., Y.C. and Y.T. The statistical analysis was completed by Z.P., Z.L., C.H.L. and C.-P.C. Data were analyzed by L.Z., P.X. and Z.P. The manuscript was written by L.Z. and P.X.

ADDITIONAL INFORMATION

Supplementary information accompanies this paper at https://doi.org/10.1038/s41422-020-00443-z.

Competing interests: The authors declare no competing interests.

REFERENCES

1. Song, M. S., Salmena, L. & Pandolfi, P. P. The functions and regulation of the PTEN tumour suppressor. *Nat. Rev. Mol. Cell Biol.* **13**, 283–296 (2012).
2. Naguib, A. et al. PTEN functions by recruitment to cytoplasmic vesicles. *Mol. Cell* **58**, 255–268 (2015).
3. Stambolic, V. et al. Negative regulation of PKB/Akt-dependent cell survival by the tumor suppressor PTEN. *Cell* **95**, 29–39 (1998).
4. Salmena, L., Carracedo, A. & Pandolfi, P. P. Tenets of PTEN tumor suppression. *Cell* **133**, 403–414 (2008).
5. Hollander, M. C., Blumenthal, G. M. & Dennis, P. A. PTEN loss in the continuum of common cancers, rare syndromes and mouse models. *Nat. Rev. Cancer* **11**, 289–301 (2011).
6. Lee, J. O. et al. Crystal structure of the PTEN tumor suppressor: implications for its phosphoinositide phosphatase activity and membrane association. *Cell* **99**, 323–334 (1999).
7. Lee, Y. R., Chen, M. & Pandolfi, P. P. The functions and regulation of the PTEN tumour suppressor: new modes and prospects. *Nat. Rev. Mol. Cell Biol.* **19**, 547–562 (2018).
8. Shen, W. H. et al. Essential role for nuclear PTEN in maintaining chromosomal integrity. *Cell* **128**, 157–170 (2007).
9. Puc, J. & Parsons, R. PTEN loss inhibits CHK1 to cause double stranded-DNA breaks in cells. *Cell Cycle* **4**, 927–929 (2005).
10. Li, A. G. et al. Mechanistic insights into maintenance of high p53 acetylation by PTEN. *Cell* **23**, 575–587 (2006).
11. Ying, H. et al. PTEN is a major tumor suppressor in pancreatic ductal adenocarcinoma and regulates an NF-κB-cytokine network. *Cancer Discov.* **1**, 158–169 (2011).
12. Wang, J. et al. Loss of tumor suppressor p53 decreases PTEN expression and enhances signaling pathways leading to activation of activator protein 1

and nuclear factor kappaB induced by UV radiation. *Cancer Res.* **65**, 6601–6611 (2005).
13. Song, M. S. et al. Immunohistochemical tumor-suppressive complex in a phosphatase-independent manner. *Cell* **144**, 187–199 (2011).
14. Trotman, L. C. et al. Ubiquitination regulates PTEN nuclear import and tumor suppression. *Cell* **128**, 141–156 (2007).
15. Song, M. S. et al. The deubiquitinylation and localization of PTEN are regulated by a HAUSP-PML network. *Nature* **455**, 813–817 (2008).
16. Bassi, C. et al. Nuclear PTEN controls DNA repair and sensitivity to genotoxic stress. *Science* **341**, 395–399 (2013).
17. Kerscher, O., Felberbaum, R. & Hochstrasser, M. Modification of proteins by ubiquitin and ubiquitin-like proteins. *Ann. Rev. Cell Dev. Biol*. **22**, 159–180 (2006).
18. Enchev, R. I., Schulman, B. A. & Peter, M. Protein neddylation: beyond cullin-RING ligases. *Nat. Rev. Mol. Cell Biol.* **16**, 30–44 (2015).
19. Mendoza, H. M. et al. NEDP1, a highly conserved cysteine protease that deNEDDylates Cullins. *J. Biol. Chem.* **278**, 25637–25643 (2003).
20. Cope, G. A. et al. Role of predicted metalloprotease motif of Jab1/Csn5 in cleavage of Nedd8 from Cul1. *Science* **298**, 608–611 (2002).
21. Soucy, T. A. et al. An inhibitor of NEDD8-activating enzyme as a new approach to treat cancer. *Nature* **458**, 732–736 (2009).
22. Abidi, N. & Xirodimas, D. P. Regulation of cancer-related pathways by protein NEDDylation and strategies for the use of NEDD8 inhibitors in the clinic. *Endocr. Relat. Cancer* **22**, T55–T70 (2015).
23. Zhou, L. & Jia, L. Targeting Protein Neddylation for Cancer Therapy. *Adv. Exp. Med. Biol.* **1217**, 297–315 (2020).
24. Finicle, B. T., Jayashankar, V. & Edinger, A. L. Nutrient scavenging in cancer. *Nat. Rev. Cancer* **18**, 619–633 (2018).
25. Hu, Q. et al. LncRNAs-directed PTEN enzymatic switch governs epithelial-mesenchymal transition. *Cell Res.* **29**, 286–304 (2019).
26. Liang, H. et al. PTENα, a PTEN isoform translated through alternative initiation, regulates mitochondrial function and energy metabolism. *Cell Metab.* **19**, 836–848 (2014).
27. Liang, H. et al. PTENβ is an alternatively translated isoform of PTEN that regulates rDNA transcription. *Nat. Commun.* **8**, 14771 (2017).
28. Xie, P. et al. The covalent modifier Nedd8 is critical for the activation of Smurf1 ubiquitin ligase in tumorigenesis. *Nat. Commun.* **5**, 3733 (2014).
29. Ohki, Y. et al. The mechanism of poly-NEDD8 chain formation in vitro. *Biochem. Biophys. Res. Commun.* **381**, 443–447 (2009).
30. Keuss, M. J. et al. Unanchored tri-NEDD8 inhibits PARP-1 to protect from oxidative stress induced cell death. *EMBO J.* **38**, e100024 (2019).
31. Hori, T. et al. Covalent modification of all members of human cullin family proteins by NEDD8. *Oncogene* **18**, 6829–6834 (1999).
32. Zhuang, M., Guan, S., Wang, H., Burlingame, A. L. & Wells, J. A. Substrates of IAP ubiquitin ligases identified with a designed orthogonal E3 ligase, the NEDDylator. *Mol. Cell* **49**, 273–282 (2013).
33. Van Themsche, C., Leblanc, V., Parent, S. & Asselin, E. X-linked inhibitor of apoptosis protein (XIAP) regulates PTEN ubiquitination, content, and compartmentalization. *J. Biol. Chem.* **284**, 20462–20466 (2009).
34. Lloyd, C. T. et al. Ubiquitination regulates PTEN nuclear import and tumor suppression. *Cell* **128**, 141–156 (2007).
35. Lee, Y. R. et al. Reactivation of PTEN tumor suppressor for cancer treatment through inhibition of a MYC-WWP1 inhibitory pathway. *Science* **364**, eaau0159 (2019).
36. Maddika, S. et al. WWP2 Is an E3 ubiquitin Ligase for PTEN. *Nat. Cell Biol.* **13**, 728–733 (2011).
37. Harper, J. W. Neddylating the guardian; Mdm2 catalyzed conjugation of Nedd8 to p53. *Cell* **118**, 2–4 (2004).
38. Zuo, W. et al. c-Cbl-mediated neddylation antagonizes ubiquitination and degradation of the TGF-β type II receptor. *Mol. Cell* **49**, 499–510 (2013).
39. Hu, J., McCall, C. M., Ohta, T. & Xiong, Y. Targeted ubiquitination of CDT1 by the DDB1 CUL4A-ROC1 ligase in response to DNA damage. *Nat. Cell Biol.* **6**, 1003–1009 (2004).
40. Nikolovska-Coleska, Z. et al. Discovery of embelin as a cell-permeable, small-molecular weight inhibitor of XIAP through structure-based computational screening of a traditional herbal medicine three-dimensional structure database. *J. Med. Chem.* **47**, 2430–2440 (2004).
41. Siegel, C., Li, J., Liu, F., Benashski, S. E. & McCullough, L. D. miR-23a regulation of X-linked inhibitor of apoptosis (XIAP) contributes to sex differences in the response to cerebral ischemia. *Proc. Natl. Acad. Sci. USA* **108**, 11662–11667 (2011).
42. Yang, J. R.-M. et al. Characterization of PTEN mutations in brain cancer reveals that Pten mono-ubiquitination promotes protein stability and nuclear localization. *Oncogene* **36**, 3673–3685 (2017).
43. Valiente, M. et al. Binding of PTEN to specific PDZ domains contributes to PTEN protein stability and phosphorylation by microtubule-associated serine/threonine kinases. *J. Biol. Chem.* **280**, 28936–28943 (2005).
44. Huang, G. et al. SCCRO (DCUN1D1) promotes nuclear translocation and assembly of the neddylation E3 complex. *J. Biol. Chem.* **286**, 10297–10304 (2012).
45. Jia, X. et al. Neddylation inactivation facilitates FOXO3a nuclear export to suppress estrogen receptor transcription and improve fulvestrant sensitivity. *Clin. Cancer Res.* **25**, 3658–3672 (2019).
46. Beck, M. & Hurt, E. The nuclear pore complex: understanding its function through structural insight. *Nat. Rev. Mol. Cell Biol.* **18**, 73–89 (2017).
47. Choudhary, C., Weinert, B. T., Nishida, Y., Verdin, E. & Mann, M. The growing landscape of lysine acetylation links metabolism and cell signalling. *Nat. Rev. Mol. Cell Biol.* **15**, 536–550 (2014).
48. Ikenoue, T., Inoki, K., Zhao, B. & Guan, K. L. PTEN acetylation modulates its interaction with PDZ domain. *Cancer Res.* **68**, 6908–6912 (2008).
49. Liu, F. et al. PTEN enters the nucleus by diffusion. *J. Cell Biochem.* **96**, 221–234 (2005).
50. Guan, J., Zhao, Q. & Mao, W. Nuclear PTEN interferes with binding of Ku70 at double-strand breaks through post-translational poly(ADP-ribosyl)ation. *Biochim. Biophys. Acta.* **1863**, 3106–3115 (2016).
51. Malaney, P., Palumbo, E., Semidey-Hurtado, J. & Hardee, J. PTEN physically Interacts with and regulates E2F1-mediated transcription in lung cancer. *Cell Cycle* **17**, 947–962 (2018).
52. Menendez, J. A. & Lupu, R. Fatty acid synthase and the lipogenic phenotype in cancer pathogenesis. *Nat. Rev. Cancer* **7**, 763–777 (2007).
53. Lin, H. P. et al. Destabilization of fatty acid synthase by acetylation inhibits de novo lipogenesis and tumor cell growth. *Cancer Res.* **76**, 6924–6936 (2016).
54. Perren, A. et al. Immunohistochemical evidence of loss of PTEN expression in primary ductal adenocarcinomas of the breast. *Am. J. Pathol.* **155**, 1253–1260 (1999).
55. Goldhirsch, A. et al. Personalizing the treatment of women with early breast cancer: highlights of the St Gallen International Expert Consensus on the Primary Therapy of Early Breast Cancer 2013. *Ann. Oncol.* **24**, 2206–2223 (2013).
56. Chen, J. H. et al. ATM-mediated PTEN phosphorylation promotes PTEN nuclear translocation and autophagy in response to DNA-damaging agents in cancer cells. *Autophagy* **11**, 239–252 (2015).
57. Wu, Y. et al. PTEN phosphorylation and nuclear export mediate free fatty acid-induced oxidative stress. *Antioxid. Redox Signal.* **20**, 1382–1395 (2014).
58. Gu, Y. et al. MLN4924, an NAE inhibitor, suppresses AKT and mTOR signaling via upregulation of REDD1 in human myeloma cells. *Blood* **123**, 3269–3276 (2014).
59. Barbier-Torres, L. et al. Stabilization of LKB1 and Akt by neddylation regulates energy metabolism in liver cancer. *Oncotarget* **6**, 2509–2523 (2015).
60. Crunkhorn, S. Breast cancer: FASN inhibitor increases survival. *Nat. Rev. Drug Discov.* **15**, 532 (2016).
61. Iwarawrah, Y. et al. Fasnall, a selective FASN inhibitor, shows potent anti-tumor activity in the MMTV-Neu model of HER2+ breast cancer. *Cell Chem. Biol.* **23**, 678–688 (2016).